A CONVERGENT EVOLVING FINITE ELEMENT METHOD WITH ARTIFICIAL TANGENTIAL MOTION FOR SURFACE EVOLUTION UNDER A PRESCRIBED VELOCITY FIELD*

GENMING BAI†, JIASHUN HU‡, AND BUYANG LI§

Abstract. A novel evolving surface finite element method, based on a novel equivalent formulation of the continuous problem, is proposed for computing the evolution of a closed hypersurface moving under a prescribed velocity field in two- and three-dimensional spaces. The method improves the mesh quality of the approximate surface by minimizing the rate of deformation using an artificial tangential motion. The transport evolution equations of the normal vector and the extrinsic Weingarten matrix are derived and coupled with the surface evolution equations to ensure stability and convergence of the numerical approximations. Optimal-order convergence of the semi-discrete evolving surface finite element method is proved for finite elements of degree $k \geq 2$. Numerical examples are provided to illustrate the convergence of the proposed method and its effectiveness in improving mesh quality on the approximate evolving surface.

Key words. Evolving surface finite element method, artificial tangential velocity, mesh property, transport equations, optimal error estimate, stability

AMS subject classifications. 35R01,65M12, 65M15, 65M60

1. Introduction.

We consider the evolution of a closed hypersurface $\Gamma(t)$ in $\mathbb{R}^d$, where $d = 2$ or 3, under a given velocity field u in $\mathbb{R}^d \times [0, T]$. The evolving surface $\Gamma(t)$ can be represented by the image of the flow map $X^u(\cdot, t) : \Gamma(0) \to \Gamma(t)$, which satisfies the equation

$$\partial_t X^u(\cdot, t) = u(X^u(\cdot, t), t) \quad \text{on } \Gamma(0) \tag{1.1}$$

for $t \in [0, T]$, subject to the initial condition $X^u(x, 0) = x$ for $x \in \Gamma(0)$. Stable and accurate numerical approximations to the surface evolution in (1.1) play fundamental roles in solving partial differential equations (PDEs) on a moving surface [18, 22, 39], as well as solving PDEs in a bulk domain with a moving boundary/interface by the arbitrary Lagrangian–Eulerian (ALE) methods [20, 23, 26, 40, 41] and Eulerian (unfitted) approaches [16, 45, 47]. Problem (1.1) is also relevant to the PDE-constrained shape optimization [29], the motion of interfaces in two-phase flows [27, 32] and fluid-structure interactions [46], where the velocity field u is unknown and needs to be solved in the bulk domain.

This paper concerns the evolving surface finite element methods (FEMs) for discretizing (1.1). As a Lagrangian method, the accuracy of an evolving surface FEM in approximating the evolution of a surface, or the solutions of PDEs on an evolving surface, can be greatly influenced by the mesh quality of the triangulation which forms the approximate surface. One of the main difficulties is that the mesh often becomes distorted as time grows unless some techniques are used to redistribute the mesh points; see [1]. In order to overcome this difficulty, Barrett, Garcke & Nürnberg introduced a fully discrete type of artificial tangential velocity which drives the mesh points to

*This work is supported in part by the Research Grants Council of Hong Kong (GRF project no. 15303022).

†Department of Applied Mathematics, The Hong Kong Polytechnic University, Hong Kong. E-mail address: genming.bai@connect.polyu.hk

‡Corresponding author. Department of Applied Mathematics, The Hong Kong Polytechnic University, Hong Kong. E-mail address: jiashun.hu@polyu.edu.hk

§Department of Applied Mathematics, The Hong Kong Polytechnic University, Hong Kong. E-mail address: buyang.li@polyu.edu.hk

move tangentially on the surface to improve the mesh quality; see [4, 5]. The method proposed by Barrett, Garcke & Nürnberg (which we refer to as the BGN method) was designed and became successful for approximating geometric flows, including mean curvature flow, Willmore flow, surface diffusion and Helfrich flow [2, 5–7] with good mesh quality. The BGN method has also been successfully applied to improve mesh quality of a stationary surface [5, Remark 4.3], and to other applications including two phase flow [11, 27], image segmentation [14], and growth of structures [8–10, 24].

An alternative approach to constructing artificial tangential velocities which could improve the mesh quality of the approximate surfaces was proposed by Elliott & Fritz in [21], where the tangental velocity is regarded as a kind of built-in reparametrization by the DeTurck flow techniques. By this approach, a family of tangential velocity for geometric flows which depends on an adjustable parameter was proposed in [21], and error estimates were established for curve shortening flow on a two-dimensional plane. The techniques were used in [3] for developing numerical methods, with rigorous error estimates, for approximating forced curve shortening flow coupled to a reaction-diffusion equation on the curve and in [44] for the finite difference discretization of the mean curvature flow with convergence proof. It is also important to mention that the improved nodal distribution can be also achieved by prescribing tangential velocity [24, 25], equilibrium of spring model [35] and the reparametrization of arc length [13, 15, 33, 42, 43].

Albeit its success in improving the mesh quality, rigorous proof of convergence of the BGN method for the various problems remains open due to the lack of explicit formulation of the tangential velocity. The available error estimates using the DeTurck flow also require the flow map to satisfy some parabolic evolution equations on the evolving curves. The development of stable numerical approximations (with rigorous stability and error estimates) for the numerical approximations to the surface evolution in (1.1) using the BGN method and the DeTurck flow techniques is still challenging.

It is known that the spatially semi-discretized BGN method ensures the equidistribution of vertices for evolving curves [5]. Recently, it was shown in [30] that the tangential velocity generated by the temporally semi-discretized version of the BGN method formally tends to (as the time stepsize tends to zero) the velocity which minimizes the following energy functional which represents the instantaneous rate of deformation:

$$\int_{\Gamma(t)} |\nabla_{\Gamma(t)} v(t)|^2 \tag{1.2}$$

under the constraint $v(t)\cdot n(t) = V(t)$, where $n(t)$ is the normal vector on $\Gamma(t)$ and $V(t)$ is the normal velocity of the surface in the corresponding geometric flow. Motivated by the above interpretation, we consider the following modified flow map, with a modified velocity v, for describing the surface evolution governed by (1.1):

$$\frac{d}{dt} X^v(\cdot,t) = v(X^v(\cdot,t),t) \qquad \text{on } \Gamma(0), \tag{1.3a}$$

$$v\cdot n = u\cdot n \qquad \text{on } \Gamma(t), \tag{1.3b}$$

$$-\Delta_\Gamma v = \kappa n \qquad \text{on } \Gamma(t). \tag{1.3c}$$

The modified velocity v determined by (1.3b)–(1.3c) is exactly the minimizer of the energy functional $\int_\Gamma |\nabla_\Gamma v|^2$ under the constraint $v\cdot n = u\cdot n$, with κ being a Lagrange multiplier in the constrained optimization problem. Therefore, the surface evolving under the modified velocity v has the same shape as the surface evolving under velocity u, but with minimal instantaneous rate of deformation at every time $t \in [0, T]$. The

novel formulation in (1.3b)–(1.3c) is regarded as a continuous limiting formulation of the BGN method with an explicit description of the tangential velocity. Thus, the approximation to (1.3) by the evolving surface FEM should reduce mesh distortion compared with the numerical approximations which directly discretize (1.1).

However, the direct application of the evolving surface FEM for (1.3) does not lead to good stability estimates. The reason is that, based on the stability and error estimates of evolving surface FEM for (1.3b)–(1.3c) in [30], the H^1-norm error in approximating v needs to be bounded by the H^1-norm error in approximating n which, however, depends on the piecewise H^2-norm error in approximating X. This dependence on the error of X (in terms of its second-order partial derivatives) is too strong to be controlled in the stability and error estimates. This difficulty is overcome in [30] by recovering n through the parabolic evolution equations of n discovered by Huisken for mean curvature flow [31] and by Kovács, Li & Lubich for Willmore flow [37]. These evolution equations of the normal vector were used to design convergent evolving surface FEMs for mean curvature flow and Willmore flow in [30, 36, 37]. However, these evolution equations highly depend on the specific geometric flows. Up to the authors' knowledge, no counterpart for the general surface evolution problem in (1.1) has been derived in literature.

The objective of this article is to design a numerically stable evolving surface FEM for solving (1.3) by establishing and utilizing the evolution equations of the normal vector n and the extrinsic Weingarten matrix $\nabla_\Gamma n$ properly, and prove the optimal convergence of the numerical approximations. In Section 2.2 we shall prove that the normal vector n on the evolving surface $\Gamma(t)$ determined by (1.3a)–(1.3c) can be recovered by solving the following two transport equations of $p : \Gamma(t) \to \mathbb{R}^d$ and $q : \Gamma(t) \to \mathbb{R}^{d\times d}$ and one elliptic equation of $n : \Gamma(t) \to \mathbb{R}^d$:

$$\partial_t^\bullet p - ((v-u)\cdot\nabla_\Gamma)\, p = -(I-pp^T)(\nabla u)p, \tag{1.3d}$$

$$\begin{aligned}\partial_t^\bullet q - ((v-u)\cdot\nabla_\Gamma)q = {} & p(v-u)^T q^2 - \sum_{j=1}^{d}(I-pp^T)\nabla^2 u_j (I-pp^T)p_j \\ & + q\nabla u pp^T + p^T\nabla u pq - q(\nabla u)^T(I-pp^T) \\ & - (I-pp^T)(\nabla u)q + pp^T(\nabla_\Gamma v)^T q,\end{aligned} \tag{1.3e}$$

$$n - \Delta_\Gamma n = p - \nabla_\Gamma \cdot q, \tag{1.3f}$$

where $p = n$ and $q = \nabla_\Gamma n$ are different notations of the normal vector and the Weingarten matrix, respectively. The key idea is that we delicately select (1.3d)–(1.3f) from their various equivalent formulations in order to have the following two advantages for the numerical approximations. On the one hand, the evolution equations (1.3d)–(1.3e) can provide full order approximation to the geometrical quantities such as the normal vector and the Weingarten matrix. On the other hand, the normal vector n obtained from (1.3f) can satisfy the following requirement: By estimating n in terms of p and q, and then estimating p and q in terms of X and v, the $L^\infty(0,t;H^1)$-norm error in approximating n from solving (1.3d)–(1.3f) can be bounded by the $L^\infty(0,t;H^1)$-norm error of X and the $L^2(0,t;H^1)$-norm error of v. In this way, the main difficulty in the stability analysis for (1.3a)–(1.3c) (i.e., the dependence on the piecewise H^2-norm error in approximating X, as mentioned in the last paragraph above) can be circumvented, and the energy estimate for transport equation can be applied after paying special attention on the integration by part argument in the framework of evolving surface FEM for piecewise smooth surfaces. Accordingly, the $L^\infty(0,t;H^1)$-norm error of X and the $L^2(0,t;H^1)$-norm error of v can be controlled in the stability estimates

by using Gronwall's inequality.

In practice, (1.3d)–(1.3f) require solving additional $d^2 + 2d$ scalar functions on evolving surface, with the computational cost comparable to solving (1.3a)–(1.3c). Therefore, the computational cost of solving (1.3a)–(1.3f) is equivalent to solving (1.3a)–(1.3c) without significant increase. In addition, the increase in computational cost will be more acceptable for typical applications such as solving PDEs in a bulk domains $\Omega(t)$ with an evolving boundary $\Gamma(t) = \partial\Omega(t)$, as the computational cost of solving the surface PDEs in (1.3a)–(1.3f) is often negligible compared with the computational cost of solving PDEs in the bulk domain. This is demonstrated in the last numerical example in Example 4.4.

The rest of this article is organized as follows. In Section 2, we introduce the basic notations and formulas to be used in the construction and analysis of the numerical method, and present the derivation of the evolution equations in (1.3d)–(1.3f). Then we present the weak formulation and the evolving surface FEM for (1.3), as well as the corresponding matrix-vector formuation for practical computation. At the end of Section 2, we present the main theorem on the convergence of the evolving surface FEM for (1.3). In Section 3, we prove the stability and convergence of the evolving surface FEM. In Section 4, we present several numerical examples to support the theoretical analysis in this article and to illustrate the effectiveness of the proposed method in improving the mesh quality of the approximate evolving surfaces. In addition, we present an example to show the capability of the proposed artificial tangential velocity in improving the effectiveness of the arbitrary Lagrangian–Eulerian method for solving PDEs on a domain with moving boundary.

2. The numerical scheme and main result. In this section, we introduce the basic notations and formulas to be used in the construction and analysis of the numerical method. By using these formulas, we derive the PDEs in (1.3d)–(1.3f) which are used to recover the normal vector n on the evolving surface, which is needed in determining the modified velocity v through (1.3a)–(1.3c). Then we present the weak formulation and evolving surface FEM for the system (1.3), as well as the main theorem on the convergence of numerical solutions.

2.1. Basic notations and formulas. It is known that for a smooth surface Γ with principle curvatures κ_i bounded by δ^{-1}, the distance projection onto Γ is well defined in a neighborhood of Γ, i.e.,

$$\Omega_\delta(\Gamma) := \{x \in \mathbb{R}^d : \operatorname{dist}(x, \Gamma) \le \delta\},$$

where $\operatorname{dist}(x, \Gamma)$ denotes the distance from x to Γ; see [28, Lemma 14.17]. Namely, for any point $\hat{x} \in \Omega_\delta(\Gamma)$, its distance projection $a(\hat{x}) \in \Gamma$ is determined by

$$a(\hat{x}) = \hat{x} - \operatorname{dist}(\hat{x}, \Gamma) n(a(\hat{x}), \Gamma), \tag{2.1}$$

with $n(a(\hat{x}), \Gamma)$ denoting the normal vector of Γ at $a(\hat{x})$. With the help of the distance projection in (2.1), one can define the normal extension of u from Γ to $\Omega_\delta(\Gamma)$ by

$$u^\ell = u \circ a. \tag{2.2}$$

The surface gradient of a scalar-valued function $\eta \in H^1(\Gamma, \mathbb{R})$ is defined as a column vector $\nabla_\Gamma \eta := (I - nn^T)(\nabla \eta^\ell)|_\Gamma$. The jth component of $\nabla_\Gamma \eta$ is denoted by $D_j \eta$. The surface gradient of a vector-valued function $\boldsymbol{\eta} \in H^1(\Gamma, \mathbb{R}^d)$ is denoted by $\nabla_\Gamma \boldsymbol{\eta} = \big(\nabla_\Gamma \boldsymbol{\eta}_1, \cdots, \nabla_\Gamma \boldsymbol{\eta}_d\big)$, with the columns being the surface gradients of the components of u. The surface Hessian of η is defined as $\nabla_\Gamma^2 \eta = \nabla_\Gamma(\nabla_\Gamma \eta)$. Following [12, Lemma 15], the surface Hessian is not symmetric. Moreover, the commutator

satisfies

$$[D_i, D_j]\eta := (D_i D_j - D_j D_i)\eta = n_i \nabla_\Gamma n_j \cdot \nabla_\Gamma \eta - n_j \nabla_\Gamma n_i \cdot \nabla_\Gamma \eta. \tag{2.3}$$

Let $A = \nabla_\Gamma n \in \mathbb{R}^{d\times d}$ denote the extrinsic Weingarten matrix.

For a function w defined on an evolving surface $\bigcup_{t\in[0,T]} \Gamma(t) \times \{t\}$, the material derivative of w with respect to the velocity of the evolving surface (1.3a) is defined as

$$\partial_t^\bullet w(X^v(x,t),t) = \frac{d}{dt} w(X^v(x,t),t), \quad x \in \Gamma(0).$$

An important relation between the surface gradient and the material derivative is the following formula (see [19, Lemma 2.6]):

$$\partial_t^\bullet \nabla_{\Gamma(t)} w = \nabla_{\Gamma(t)}(\partial_t^\bullet w) - (\nabla_{\Gamma(t)} v - n_{\Gamma(t)} n_{\Gamma(t)}^T (\nabla_{\Gamma(t)} v)^T)\nabla_{\Gamma(t)} w. \tag{2.4}$$

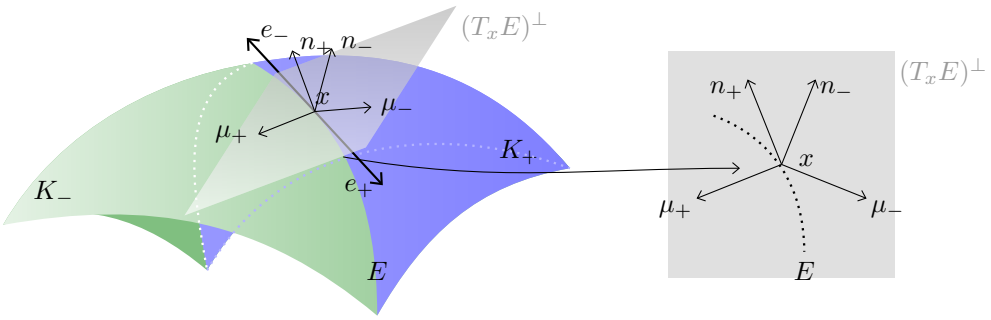

Fig. 2.1. *Illustration of $n_\pm$ and $\mu_\pm$, which lie in the same plane $(T_xE)^\perp$.*

Next, we introduce the Stokes theorem on a closed, globally continuous piecewise smooth surface $\Gamma_h = \bigcup_i \Gamma_{h,i}$ composed of smooth elements $\Gamma_{h,i}$. We denote by $\mathcal{E}$ the collection of common edges of adjacent smooth pieces, and denote by P_τ and H the piecewise-defined tangential projection and mean curvature of Γ_h, respectively.

Let $E \in \mathcal{E}$ be a common edge of two adjacent elements K_+ and K_- as illustrated in Figure 2.1. Induced by the outward normal vectors $n_\pm$, the orientations of E as boundary of $K_\pm$ are indicated by unit vectors $e_\pm$. The outward conormal vectors $\mu_\pm$ are defined by $\mu_\pm = e_\pm \times n_\pm$ on E. The jump of μ at E is defined as $[\mu]_E = \mu_+ + \mu_-$. Since $e_+ + e_- = 0$, we deduce

$$[\mu]_E = e_+ \times (n_+ - n_-). \tag{2.5}$$

Suppose $n_\pm$ are close enough so that $n_+ + n_-$ is nonzero, we denote the unit angle bisector direction of $n_\pm$ as $\hat{n} := (n_+ + n_-)/|n_+ + n_-|$. It is easy to verify that $[\mu]_E$ is parallel to $\hat{n}$, i.e.,

$$[\mu]_E = \pm |[\mu]_E| \hat{n}. \tag{2.6}$$

For $\boldsymbol{\eta} \in H^1(\Gamma_h, \mathbb{R}^d)$, by applying the Stokes theorem on each smooth $\Gamma_{h,i}$ (see [18, (2.2)]) and summing over all smooth pieces, we derive

$$\int_{\Gamma_h} \nabla_{\Gamma_h} \cdot \boldsymbol{\eta} = \sum_{E\in\mathcal{E}} \int_E \boldsymbol{\eta} \cdot [\mu]_E + \int_{\Gamma_h} H(\boldsymbol{\eta} \cdot n). \tag{2.7}$$

The following formula is derived directly.

$$\int_{\Gamma_h}((v\cdot\nabla_{\Gamma_h})\boldsymbol{\eta})\cdot\boldsymbol{\eta}=\frac{1}{2}\left[\sum_{E\in\mathcal{E}}\int_E|\boldsymbol{\eta}|^2v\cdot[\mu]_E+\int_{\Gamma_h}|\boldsymbol{\eta}|^2\big[H(v\cdot n)-(\nabla_{\Gamma_h}\cdot v)\big]\right]. \quad (2.8)$$

2.2. Derivation of (1.3d)–(1.3f)**.** For the evolving hypersurface $\Gamma(t)$ with velocity field v, following [12, Lemma 37], the evolution of n is described by

$$\partial_t^\bullet n=-(\nabla_\Gamma v)n, \quad (2.9)$$

which can be reformulated into a nonlinear perturbation of a transport equation by using (1.3b) and the Leibniz rule,

$$\partial_t^\bullet n=-(\nabla_\Gamma(v-u))n-(\nabla_\Gamma u)n=((v-u)\cdot\nabla_\Gamma)\,n-(I-nn^T)(\nabla u)n, \quad (2.10)$$

where the last equality uses the relation $(v-u)\cdot n=0$ and the symmetry of $\nabla_\Gamma n$. Equation (2.10) is exactly the evolution equation in (1.3d) with the notation $p=n$.

By Leibniz rule, we have

$$D_i((v-u)_jD_jn)=D_i(v-u)_jD_jn+(v-u)_jD_jD_in+(v-u)_j[D_i,D_j]n,$$

together with (2.3), $(u-v)\cdot n=0$ and $A=\nabla_\Gamma n$, we obtain

$$\nabla_\Gamma(((v-u)\cdot\nabla_\Gamma)n)=\nabla_\Gamma(v-u)A+((v-u)\cdot\nabla_\Gamma)A+n(v-u)^TA^2. \quad (2.11)$$

Similarly, we can obtain

$$\nabla_\Gamma^2u_k=(I-nn^T)\nabla^2u_k(I-nn^T)-A\nabla_\Gamma u_kn^T-n^T\nabla_\Gamma u_kA. \quad (2.12)$$

By taking surface gradient of (2.10) and using the identities in (2.11)–(2.12), we obtain

$$\begin{aligned}\nabla_\Gamma\partial_t^\bullet n=&\nabla_\Gamma(v-u)A+((v-u)\cdot\nabla_\Gamma)A+n(v-u)^TA^2-A(\nabla_\Gamma u)^T\\&-n_i\left((I-nn^T)\nabla^2u_i(I-nn^T)-A\nabla u_in^T-n^T\nabla u_iA\right). \quad (2.13)\end{aligned}$$

Then, combining (2.4) and (2.13), we obtain the following evolution equation for A:

$$\begin{aligned}\partial_t^\bullet A=&((v-u)\cdot\nabla_\Gamma)A+n(v-u)^TA^2-\sum_{j=1}^d(I-nn^T)\nabla^2u_j(I-nn^T)n_j\\&+A\nabla unn^T+n^T\nabla unA-A(\nabla u)^T(I-nn^T)\\&-(I-nn^T)(\nabla u)A+nn^T(\nabla_\Gamma v)^TA. \quad (2.14)\end{aligned}$$

Equation (1.3e) is obtained by replacing n and A by p and q in (2.14), respectively.

Since $p=n$ and $q=\nabla_\Gamma n$, it follows that $n-\Delta_\Gamma n=p-\nabla_\Gamma\cdot q$. This proves (1.3f).

For later convenience, let us denote $U=(u_l,\partial_{x_i}u_l,\partial_{x_ix_j}u_l)_{i,j,l=1,\cdots,d}\in\mathbb{R}^{d+d^2+d^3}$ and introduce smooth functions,

$$\begin{aligned}g(U,p,q,v,\nabla_\Gamma v)=&\,p(v-u)^Tq^2-q(\nabla u)^T(I-pp^T)-(I-pp^T)(\nabla u)q+q\nabla upp^T\\&+p^T\nabla upq+pp^T(\nabla_\Gamma v)^Tq-\sum_{j=1}^d(I-pp^T)\nabla^2u_j(I-pp^T)p_j, \quad (2.15)\end{aligned}$$

$$f(U,p)=-(I-pp^T)(\nabla u)p. \quad (2.16)$$

2.3. The evolving surface finite element discretization. Given a closed smooth initial surface $\Gamma(0)\subset\mathbb{R}^d$ and its admissible family of shape-regular and quasi-uniform (see [18]) triangulations $\mathcal{T}_h$ with mesh size h, an isoparametric finite element space $S_h[\mathbf{x}(0)]$ of degree k can be defined on the piecewise polynomial approximate surface $\Gamma_h[\mathbf{x}(0)]$ as in [17], where $\mathbf{x}(0)=(x_1,\cdots,x_N)\in\mathbb{R}^{3N}$ collects all nodes $x_j\in\Gamma(0)$

that correspond to the degrees of freedom of $S_h[\mathbf{x}(0)]$. With respect to the discretized velocity $v_h(t) \in S_h[\mathbf{x}(0)]$, the evolution of $\mathbf{x}(0)$ determines $\mathbf{x}(t) = (x_1(t), \cdots, x_N(t))$ and consequently the evolving approximate surface $\Gamma_h[\mathbf{x}(t)]$, which is represented by a unique finite element function $X_h(\cdot, t) \in S_h[\mathbf{x}(0)]$ (the discrete flow map) satisfying

$$X_h(x_j, t) = x_j(t), \quad \forall\, j = 1, \ldots, N.$$

Then, the material derivative $\partial^\bullet_{t,h}$ of u_h defined on $\cup_{t\in[0,T]}\Gamma_h(t) \times \{t\}$ is defined as

$$\partial^\bullet_{t,h} u_h(y, t) = \frac{d}{dt} u_h(X_h(x, t), t), \quad \forall\, y = X_h(x, t) \in \Gamma_h[\mathbf{x}(t)].$$

The finite element basis functions of $S_h[\mathbf{x}(t)]$ are denoted by $\phi_j[\mathbf{x}(t)], j = 1, \ldots, N$, which are pull backs of $\phi_j[\mathbf{x}(0)]$ by the discrete flow map and satisfy the following identities:

$$\phi_j[\mathbf{x}(t)]\,(x_i(t)) = \delta_{ij}, \quad \partial^\bullet_{t,h}\phi_j[\mathbf{x}(t)] = 0, \quad i, j = 1, \ldots, N. \tag{2.17}$$

With $\langle\cdot,\cdot\rangle_{\Gamma_h}$ denoting the L^2 inner product on Γ_h, the evolving surface FEM for solving (1.3) is to seek $X_h \in S_h[\mathbf{x}(0)]^d$ and

$$(v_h, \kappa_h, n_h, p_h, q_h) \in S_h[\mathbf{x}(t)]^d \times S_h[\mathbf{x}(t)] \times S_h[\mathbf{x}(t)]^d \times S_h[\mathbf{x}(t)]^d \times S_h[\mathbf{x}(t)]^{d\times d}$$

such that

$$\partial_t X_h(x, t) = v_h \circ X_h(x, t) \tag{2.18a}$$
$$\langle v_h \cdot n_h, \chi_\kappa\rangle_{\Gamma_h} = \langle u \cdot n_h, \chi_\kappa\rangle_{\Gamma_h} \tag{2.18b}$$
$$\langle \nabla_{\Gamma_h} v_h, \nabla_{\Gamma_h}\chi_v\rangle_{\Gamma_h} = -\langle \kappa_h n_h, \chi_v\rangle_{\Gamma_h} \tag{2.18c}$$
$$\langle \partial^\bullet_{t,h} p_h, \chi_p\rangle_{\Gamma_h} - \langle((v_h - u)\cdot\nabla_{\Gamma_h})p_h, \chi_p\rangle_{\Gamma_h} = \langle f(U, p_h), \chi_p\rangle_{\Gamma_h} \tag{2.18d}$$
$$\langle \partial^\bullet_{t,h} q_h, \chi_q\rangle_{\Gamma_h} - \langle((v_h - u)\cdot\nabla_{\Gamma_h})q_h, \chi_q\rangle_{\Gamma_h} = \langle g(U, p_h, q_h, v_h, \nabla_{\Gamma_h} v_h), \chi_q\rangle_{\Gamma_h} \tag{2.18e}$$
$$\langle n_h, \chi_n\rangle_{\Gamma_h} + \langle \nabla_{\Gamma_h} n_h, \nabla_{\Gamma_h}\chi_n\rangle_{\Gamma_h} = \langle p_h, \chi_n\rangle_{\Gamma_h} + \langle q_h, \nabla_{\Gamma_h}\chi_n\rangle_{\Gamma_h}, \tag{2.18f}$$

hold for all test functions

$$(\chi_v, \chi_\kappa, \chi_n, \chi_p, \chi_q) \in S_h[\mathbf{x}(t)]^d \times S_h[\mathbf{x}(t)] \times S_h[\mathbf{x}(t)]^d \times S_h[\mathbf{x}(t)]^d \times S_h[\mathbf{x}(t)]^{d\times d}.$$

Remark 2.1. (2.18a)–(2.18c) can be used independently after choosing n_h as the geometrical normal vector field of Γ_h, i.e, solving velocity by

$$\langle v_h \cdot n_h, \chi_\kappa\rangle^h_{\Gamma_h} = \langle u \cdot n_h, \chi_\kappa\rangle_{\Gamma_h} \tag{2.19a}$$
$$\langle \nabla_{\Gamma_h} v_h, \nabla_{\Gamma_h}\chi_v\rangle_{\Gamma_h} = -\langle \kappa_h n_h, \chi_v\rangle^h_{\Gamma_h}, \tag{2.19b}$$

where $\langle\cdot,\cdot\rangle^h_{\Gamma_h}$ denotes the mass lumping inner product. In the numerical experiments of Section 4 (i.e., Example 4.2), we can see that Scheme (2.19) may improve the mesh distribution on a surface but has lower accuracy than (2.18) for high-order finite elements. Theoretically, it is also difficult to prove the stability and convergence of (2.19) to the solution of (1.3b)–(1.3c).

The initial values for (2.18) are chosen as follows. Given the initial isoparametric interpolated surface $\Gamma_h[\mathbf{x}(0)]$, we choose $X_h(\cdot, 0) = \mathrm{id}|_{\Gamma_h[\mathbf{x}(0)]}$. The initial values for p_h and q_h are set as the Lagrange interpolations of the exact functions. The error estimates for the Lagrange interpolation guarantee the following result (see [17]):

$$\|p^\ell_h(0) - p(0)\|_{L^2(\Gamma(0))} + \|q^\ell_h(0) - q(0)\|_{L^2(\Gamma(0))} \lesssim h^{k+1}, \tag{2.20}$$

where we have used notation $a \lesssim b$ to standard for the statement "$a \le Cb$ for some constant C which is independent of h".

2.4. Matrix-vector formulation. In this section, we follow [36, 38] to rewrite (2.18a)–(2.18f) into a matrix-vector formulation. We denote by $\mathbf{n}$, $\mathbf{v}$, $\mathbf{p}$ and $\mathbf{q}$ the vectors that collect the nodal values of n_h, v_h, p_h and q_h respectively. Since p_h and q_h are defined on $\Gamma_h[\mathbf{x}(t)]$ and take values in $\mathbb{R}^d$ and $\mathbb{R}^{d\times d}$ separately, we explicitly write down the entries of $\mathbf{p}$ and $\mathbf{q}$. For $i \le N$, $k, \ell \le d$,

$$\mathbf{p}_{(i-1)d+\ell} = (p_h(X_h(x_i,t)))_\ell, \quad \mathbf{q}_{(i-1)d^2+(k-1)d+\ell} = (q_h(X_h(x_i,t)))_{k,\ell}.$$

The mass and stiff matrices corresponding to the finite element space $S_h[\mathbf{x}(t)]$ are defined with the following entries, for $i, j \le N$,

$$\mathbf{M}_{ij}(\mathbf{x}) = \int_{\Gamma_h[\mathbf{x}]} \phi_i[\mathbf{x}]\phi_j[\mathbf{x}], \quad \mathbf{A}_{ij}(\mathbf{x}) = \int_{\Gamma_h[\mathbf{x}]} \nabla_{\Gamma_h[\mathbf{x}]}\phi_i[\mathbf{x}] \cdot \nabla_{\Gamma_h[\mathbf{x}]}\phi_j[\mathbf{x}]. \tag{2.21}$$

Let $\mathbf{K}(\mathbf{x}) = \mathbf{M}(\mathbf{x}) + \mathbf{A}(\mathbf{x})$. Define $\mathbf{B}(\mathbf{x},\mathbf{n}) \in \mathbb{R}^{N\times dN}$ and $\mathbf{E}(\mathbf{x},\mathbf{v}) \in \mathbb{R}^{N\times N}$ by

$$\mathbf{B}_{i,(j-1)d+m}(\mathbf{x},\mathbf{n}) = \int_{\Gamma_h[\mathbf{x}]} \phi_i\phi_j(n_h)_m, \quad 1 \le m \le d, \tag{2.22}$$

$$\mathbf{E}_{ij}(\mathbf{x},\mathbf{v}) = \int_{\Gamma_h[\mathbf{x}]} ((v_h - u)\cdot\nabla_{\Gamma_h[\mathbf{x}]})\phi_j \cdot \phi_i. \tag{2.23}$$

Let I_d be the $d\times d$ identity matrix and let $\otimes$ denote the kronecker product, we introduce

$$\mathbf{M}^{[d]}(\mathbf{x}) = \mathbf{M}(\mathbf{x}) \otimes I_d, \quad \mathbf{A}^{[d]}(\mathbf{x}) = \mathbf{A}(\mathbf{x}) \otimes I_d, \quad \mathbf{E}^{[d]}(\mathbf{x},\mathbf{v}) = \mathbf{E}(\mathbf{x},\mathbf{v}) \otimes I_d.$$

We define the nodal vectors $\mathbf{g}(\mathbf{x},\mathbf{p},\mathbf{v},\mathbf{q}) \in \mathbb{R}^{N\times d^2}$, $\mathbf{f}(\mathbf{x},\mathbf{p}) \in \mathbb{R}^{N\times d}$, $\mathbf{F}(\mathbf{x},\mathbf{q}) \in \mathbb{R}^{N\times d}$ and the normal velocity $\mathbf{V}(\mathbf{x},\mathbf{n}) \in \mathbb{R}^N$ by requiring for $\boldsymbol{\chi}_\mathbf{q} \in \mathbb{R}^{N\times d^2}$, $\boldsymbol{\chi}_\mathbf{p}, \boldsymbol{\chi}_\mathbf{n} \in \mathbb{R}^{N\times d}$ and $\boldsymbol{\chi} \in \mathbb{R}^N$,

$$\boldsymbol{\chi}_\mathbf{q}^T\mathbf{g}(\mathbf{x},\mathbf{p},\mathbf{v},\mathbf{q}) = \langle g(U,p_h,q_h,v_h,\nabla_{\Gamma_h}v_h),\chi_q\rangle_{\Gamma_h[\mathbf{x}]}, \tag{2.24}$$

$$\boldsymbol{\chi}_\mathbf{p}^T\mathbf{f}(\mathbf{x},\mathbf{p}) = \langle f(U,p_h),\chi_p\rangle_{\Gamma_h[\mathbf{x}]}, \tag{2.25}$$

$$\boldsymbol{\chi}_\mathbf{n}^T\mathbf{F}(\mathbf{x},\mathbf{q}) = \langle q_h,\nabla_{\Gamma_h}\chi_n\rangle_{\Gamma_h[\mathbf{x}]}, \tag{2.26}$$

$$\boldsymbol{\chi}^T\mathbf{V}(\mathbf{x},\mathbf{n}) = \langle u\cdot n_h,\chi\rangle_{\Gamma_h[\mathbf{x}]}. \tag{2.27}$$

The matrix-vector form of (2.18) can be formulated as follows,

$$\dot{\mathbf{x}} = \mathbf{v}, \tag{2.28a}$$

$$\mathbf{B}(\mathbf{x},\mathbf{n})\mathbf{v} = \mathbf{M}(\mathbf{x})\mathbf{V}(\mathbf{x},\mathbf{n}), \tag{2.28b}$$

$$\mathbf{B}(\mathbf{x},\mathbf{n})^T\boldsymbol{\kappa} + \mathbf{A}^{[d]}(\mathbf{x})\mathbf{v} = 0, \tag{2.28c}$$

$$\mathbf{M}^{[d]}(\mathbf{x})\dot{\mathbf{p}} - \mathbf{E}^{[d]}(\mathbf{x},\mathbf{v})\mathbf{p} = \mathbf{f}(\mathbf{x},\mathbf{p}), \tag{2.28d}$$

$$\mathbf{M}^{[d^2]}(\mathbf{x})\dot{\mathbf{q}} - \mathbf{E}^{[d^2]}(\mathbf{x},\mathbf{v})\mathbf{q} = \mathbf{g}(\mathbf{x},\mathbf{p},\mathbf{v},\mathbf{q}), \tag{2.28e}$$

$$\mathbf{M}^{[d]}(\mathbf{x})\mathbf{n} + \mathbf{A}^{[d]}(\mathbf{x})\mathbf{n} = \mathbf{M}^{[d]}(\mathbf{x})\mathbf{p} + \mathbf{F}(\mathbf{x},\mathbf{q}). \tag{2.28f}$$

The superscripts of d will be omitted in later discussion for the sake of brevity.

2.5. Convergence of the numerical approximations. Let $X_h^*(\cdot,t) \in S_h[\mathbf{x}(0)]$ be the interpolation of the smooth flow map $X(\cdot,t) : \Gamma(0) \to \mathbb{R}^d$. We introduce the interpolated surface $\Gamma_h^*(t)$, which is the finite element surface determined by the interpolated flow map $X_h^v(\cdot,t) \in S_h[\mathbf{x}(0)]$.

For a smooth evolving surface (thus the curvature is bounded uniformly with respect to $t \in [0,T]$), there exists a sufficiently small constant $h_0 > 0$ such that for $h \le h_0$ the interpolated surface satisfies $\Gamma_h^*(t) \subset \Omega_\delta(t)$ for all $t \in [0,T]$. For any finite element function $f_h \in S_h[\mathbf{x}(t)]$, we first identify f_h as an element in $S_h[\mathbf{x}^*(t)]$ through

nodal vectors, and then lift it as in (2.2) into a function f_h^L defined on $\Gamma(t)$.

The main theoretical result of this article is the following theorem.

Theorem 2.1. *We assume that the vector field u and the solution (X, v, κ, p, q, n) of (1.3) are sufficiently smooth for $t \in [0,T]$. In particular, the flow map $X : \Gamma^0 \times [0,T] \to \mathbb{R}^3$ and its inverse map $X(\cdot,t)^{-1} : \Gamma(t) \to \Gamma^0$ are both sufficiently smooth, uniformly with respect to $t \in [0,T]$. Then there exists a constant $h_0 > 0$ such that, for initial triangulations which are shape regular and quasi-uniform with mesh size $h \le h_0$, the solutions to the evolving surface FEM in (2.18) with finite elements of degree $k \ge 2$ satisfy the following error bounds,*

$$\begin{aligned}
&\|\mathrm{Id}^L_{\Gamma_h(t)} - \mathrm{Id}_{\Gamma(t)}\|_{H^1(\Gamma(t))^d} \lesssim h^k, \quad \|X_h^\ell(\cdot,t) - X(\cdot,t)\|_{H^1(\Gamma^0)^d} \lesssim h^k,\\
&\|v_h^L(\cdot,t) - v(\cdot,t)\|_{H^1(\Gamma(t))^d} \lesssim h^k, \quad \|n_h^L(\cdot,t) - n(\cdot,t)\|_{H^1(\Gamma(t))^d} \lesssim h^k,\\
&\|p_h^L(\cdot,t) - n(\cdot,t)\|_{L^2(\Gamma(t))^d} \lesssim h^k, \quad \|q_h^L(\cdot,t) - \nabla_\Gamma n(\cdot,t)\|_{L^2(\Gamma(t))^{d^2}} \lesssim h^k.
\end{aligned}$$

3. Proof of Theorem 2.1.

3.1. Error and Defect. Let $\mathbf{x}^*(t)$ be the nodal vector that collects the position of $\Gamma_h^*(t)$. We denote the position error by $\mathbf{e}_\mathbf{x}(t) = \mathbf{x}(t) - \mathbf{x}^*(t)$. Let $\mathbf{v}^*(t)$ denote the nodal vector of $v_h^*(t)$, which is the Ritz projection of $v(t)$ defined by requiring

$$\langle v_h^*(t), \chi_v\rangle_{\Gamma_h^*(t)} + \langle \nabla_{\Gamma_h^*} v_h^*(t), \nabla_{\Gamma_h^*}\chi_v\rangle_{\Gamma_h^*(t)} = \langle v(t), \chi_v^\ell\rangle_{\Gamma(t)} + \langle \nabla_\Gamma v(t), \nabla_\Gamma \chi_v^\ell\rangle_{\Gamma(t)}, \quad (3.1)$$

for all $\chi_v \in S_h[\mathbf{x}(t)]^d$. The error bounds for Ritz projection follow from [34, Theorem 6.3],

$$\|v_h^{*,\ell} - v\|_{L^2(\Gamma)} + h(\|v_h^{*,\ell} - v\|_{H^1(\Gamma)} + \|v_h^{*,\ell} - v\|_{L^\infty(\Gamma)}) \lesssim h^{k+1}\|v\|_{H^{k+1}(\Gamma)}. \quad (3.2)$$

Let κ_h^*, p_h^*, q_h^* and n_h^* be the Lagrange interpolations of the exact κ, p, q and n and let $\boldsymbol{\kappa}^*$, $\mathbf{p}^*$, $\mathbf{q}^*$, $\mathbf{n}^*$ collect the corresponding nodal values. The nodal errors are denoted as $\mathbf{e_v} = \mathbf{v} - \mathbf{v}^*, \mathbf{e}_{\boldsymbol{\kappa}} = \boldsymbol{\kappa} - \boldsymbol{\kappa}^*, \mathbf{e_p} = \mathbf{p} - \mathbf{p}^*, \mathbf{e_q} = \mathbf{q} - \mathbf{q}^*$, $\mathbf{e_n} = \mathbf{n} - \mathbf{n}^*, \mathbf{e_V} = \mathbf{V}(\mathbf{x},\mathbf{n}) - \mathbf{V}(\mathbf{x}^*,\mathbf{n}^*)$. The consistency errors $\mathbf{d_v} \in \mathbb{R}^N$, $\mathbf{d}_{\boldsymbol{\kappa}}, \mathbf{d_p}, \mathbf{d_n} \in \mathbb{R}^{dN}$ and $\mathbf{d_q} \in \mathbb{R}^{d^2N}$ are defined by requiring for $\boldsymbol{\chi}_{\boldsymbol{\kappa}} \in \mathbb{R}^N$, $\boldsymbol{\chi}_\mathbf{v}, \boldsymbol{\chi}_\mathbf{p}, \boldsymbol{\chi}_\mathbf{n} \in \mathbb{R}^{dN}$ and $\boldsymbol{\chi}_\mathbf{q} \in \mathbb{R}^{d^2N}$,

$$\boldsymbol{\chi}_{\boldsymbol{\kappa}}^T\mathbf{M}^*\mathbf{d_v} = \langle v_h^*\cdot n_h^*, \chi_\kappa\rangle_{\Gamma_h^*} - \langle u\cdot n_h^*, \chi_\kappa\rangle_{\Gamma_h^*}, \quad (3.3)$$

$$\boldsymbol{\chi}_\mathbf{v}^T\mathbf{M}^*\mathbf{d}_{\boldsymbol{\kappa}} = \langle \kappa_h^* n_h^*, \chi_v\rangle_{\Gamma_h^*} + \langle \nabla_{\Gamma_h^*} v_h^*, \nabla_{\Gamma_h^*}\chi_v\rangle_{\Gamma_h^*}, \quad (3.4)$$

$$\boldsymbol{\chi}_\mathbf{p}^T\mathbf{M}^*\mathbf{d_p} = \langle \partial_{t,h}^\bullet p_h^* - ((v_h^* - u)\cdot\nabla_{\Gamma_h^*})p_h^* - f(U, p_h^*), \chi_p\rangle_{\Gamma_h^*}, \quad (3.5)$$

$$\boldsymbol{\chi}_\mathbf{q}^T\mathbf{M}^*\mathbf{d_q} = \langle \partial_{t,h}^\bullet q_h^* - ((v_h^* - u)\cdot\nabla_{\Gamma_h^*})q_h^* - g(U, p_h^*, q_h^*, v_h^*, \nabla_{\Gamma_h^*}v_h^*), \chi_q\rangle_{\Gamma_h^*}, \quad (3.6)$$

$$\boldsymbol{\chi}_\mathbf{n}^T\mathbf{M}^*\mathbf{d_n} = \langle n_h^* - p_h^*, \chi_n\rangle_{\Gamma_h^*} + \langle \nabla_{\Gamma_h^*} n_h^* - q_h^*, \nabla_{\Gamma_h^*}\chi_n\rangle_{\Gamma_h^*}. \quad (3.7)$$

Error equations are obtained as follows,

$$\mathbf{B}^*\mathbf{e_v} = (\mathbf{B}^* - \mathbf{B})\mathbf{v} + \mathbf{M}^*\mathbf{e_V} - (\mathbf{M}^* - \mathbf{M})\mathbf{V} - \mathbf{M}^*\mathbf{d_v}, \quad (3.8a)$$

$$(\mathbf{B}^*)^T\mathbf{e}_{\boldsymbol{\kappa}} + \mathbf{A}^*\mathbf{e_v} = ((\mathbf{B}^*)^T - \mathbf{B}^T)\boldsymbol{\kappa} + (\mathbf{A}^* - \mathbf{A})\mathbf{v} - \mathbf{M}^*\mathbf{d}_{\boldsymbol{\kappa}}, \quad (3.8b)$$

$$\mathbf{M}\dot{\mathbf{e}}_\mathbf{p} + \mathbf{E}^*\mathbf{p}^* - \mathbf{E}\mathbf{p} = (\mathbf{M}^* - \mathbf{M})\dot{\mathbf{p}}^* + \mathbf{f}(\mathbf{x},\mathbf{p}) - \mathbf{f}(\mathbf{x}^*,\mathbf{p}^*) - \mathbf{M}^*\mathbf{d_p}, \quad (3.8c)$$

$$\mathbf{M}\dot{\mathbf{e}}_\mathbf{q} + \mathbf{E}^*\mathbf{q}^* - \mathbf{E}\mathbf{q} = (\mathbf{M}^* - \mathbf{M})\dot{\mathbf{q}}^* + \mathbf{g}(\mathbf{x},\mathbf{p},\mathbf{v},\mathbf{q}) - \mathbf{g}(\mathbf{x}^*,\mathbf{p}^*,\mathbf{v}^*,\mathbf{q}^*) - \mathbf{M}^*\mathbf{d_q}, \quad (3.8d)$$

$$\mathbf{K}\mathbf{e_n} - \mathbf{M}\mathbf{e_p} = (\mathbf{K}^* - \mathbf{K})\mathbf{n}^* - (\mathbf{M}^* - \mathbf{M})\mathbf{p}^* + \mathbf{F}(\mathbf{x},\mathbf{q}) - \mathbf{F}(\mathbf{x}^*,\mathbf{q}^*) - \mathbf{M}^*\mathbf{d_n}. \quad (3.8e)$$

3.2. Geometric estimates on the intermediate surface. In this section, we recall some bilinear estimates in [36, 38] concerning $\mathbf{M}^* - \mathbf{M}$ and $\mathbf{A}^* - \mathbf{A}$ in (3.8).

Their proofs are based on the intermediate surface between Γ_h and Γ_h^* . Let Γ_h^θ be a finite element surface with nodal vector $\mathbf{x}^\theta = \mathbf{x}^* + \theta \mathbf{e}_{\mathbf{x}}$. As θ varies, the velocity field $e_x^\theta \in S_h[\mathbf{x}^\theta]$ generates a map $b_\theta : \Gamma_h^0 = \Gamma_h^* \to \Gamma_h^\theta$. The material derivative is defined by

$$\partial_\theta^\bullet f(b_\theta(p)) = \frac{d}{ds}|_{s=\theta} f(b_s(p)), \quad \forall p \in \Gamma_h^*.$$

Given a nodal vector $\mathbf{w}$, we can define finite element functions $w_h^\theta \in S_h[\mathbf{x}^\theta]$ such that $\partial_\theta^\bullet w_h^\theta = 0$. It is known that

$$\begin{aligned}
\|\mathbf{w}\|^2_{\mathbf{M}(\mathbf{x})} &= \mathbf{w}^T \mathbf{M}(\mathbf{x}) \mathbf{w} = \|w_h\|^2_{L^2(\Gamma_h[\mathbf{x}])}, \\
\|\mathbf{w}\|^2_{\mathbf{A}(\mathbf{x})} &= \mathbf{w}^T \mathbf{A}(\mathbf{x}) \mathbf{w} = \left\|\nabla_{\Gamma_h[\mathbf{x}]} w_h\right\|^2_{L^2(\Gamma_h[\mathbf{x}])}, \\
\|\mathbf{w}\|^2_{\mathbf{K}(\mathbf{x})} &= \mathbf{w}^T \mathbf{K}(\mathbf{x}) \mathbf{w} = \|w_h\|^2_{H^1(\Gamma_h[\mathbf{x}])}, \\
\|\mathbf{w}\|^2_{*,\mathbf{x}} &= \mathbf{w}^T \mathbf{M}(\mathbf{x}) \mathbf{K}(\mathbf{x})^{-1} \mathbf{M}(\mathbf{x}) \mathbf{w} = \|w_h\|_{H_h^{-1}(\Gamma_h[\mathbf{x}])}.
\end{aligned}$$

According to [36, Lemma 7.2 and (7.7)], when the following condition is satisfied,

$$\|\nabla_{\Gamma_h^*} e_x^0\|_{L^\infty(\Gamma_h^*)} \le 1/4, \tag{3.9}$$

then

$$\begin{aligned}
&\|\mathbf{w}\|_{\mathbf{M}(\mathbf{x}^\theta)} \text{ is } h\text{-uniformly equivalent for } \theta \in [0,1], \\
&\text{so are the norms } \|\mathbf{w}\|_{\mathbf{A}(\mathbf{x}^\theta)} \text{ and } \|\nabla_{\Gamma_h^\theta} w_h^\theta\|_{L^\infty(\Gamma_h^\theta)}.
\end{aligned} \tag{3.10}$$

The following results can be directly obtained from [38, Lemma 4.1].

Lemma 3.1. *Suppose that condition* (3.9) *is satisfied. Then,*

$$\mathbf{z}^T(\mathbf{M} - \mathbf{M}^*)\mathbf{w} \lesssim \|\mathbf{z}\|_{\mathbf{M}^*} \|\mathbf{e}_{\mathbf{x}}\|_{\mathbf{A}^*} \|w_h^0\|_{L^\infty(\Gamma_h^*)}, \tag{3.11}$$

$$\mathbf{z}^T(\mathbf{A} - \mathbf{A}^*)\mathbf{w} \lesssim \|\mathbf{z}\|_{\mathbf{A}^*} \|\mathbf{e}_{\mathbf{x}}\|_{\mathbf{A}^*} \|\nabla_{\Gamma_h^*} w_h^0\|_{L^\infty(\Gamma_h^*)}. \tag{3.12}$$

The following lemma estimates some important geometric quantities on Γ_h^θ including the normal, the piecewisely defined mean curvature $H_{\Gamma_h^\theta}$ and jump of conormal.

Lemma 3.2. *Suppose that condition* (3.9) *is satisfied. Then,*

$$\|\partial_\theta^\bullet n_{\Gamma_h^\theta}\|_{L^\infty(\Gamma_h^\theta)} \lesssim \|\nabla_{\Gamma_h^*} e_x^0\|_{L^\infty(\Gamma_h^*)}. \tag{3.13}$$

Furthermore, there exists $h_0 > 0$ such that for $h \le h_0$, we have

$$\|H_{\Gamma_h^\theta}\|_{L^\infty(\Gamma_h^\theta)} \lesssim 1 + h^{-1} \|\nabla_{\Gamma_h^*} e_x^0\|_{L^\infty(\Gamma_h^*)}, \tag{3.14}$$

$$\|\partial_\theta^\bullet |[\mu]|\|_{L^\infty(E^\theta)} \lesssim \|\nabla_{\Gamma_h^*} e_x^0\|_{L^\infty(\Gamma_h^*)}, \quad \|[\mu]\|_{L^\infty(E^\theta)} \lesssim h^k + \|\nabla_{\Gamma_h^*} e_x^0\|_{L^\infty(\Gamma_h^*)}. \tag{3.15}$$

Proof. The first inequality (3.13) has been proved in [38, Lemma 4.5] and it can be directly obtained from the following analogy of (2.9),

$$\partial_\theta^\bullet n_{\Gamma_h^\theta} = -(\nabla_{\Gamma_h^\theta} e_x^\theta) n_{\Gamma_h^\theta}. \tag{3.16}$$

Applying surface gradient to (3.16) and using (2.4) yield

$$\partial_\theta^\bullet A^\theta = -\sum_{i=1}^d \nabla^2_{\Gamma_h^\theta} e^\theta_{x\,i} n_{\Gamma_h^\theta\, i} - A^\theta (\nabla_{\Gamma_h^\theta} e_x^\theta)^T - (\nabla_{\Gamma_h^\theta} e_x^\theta - (n_{\Gamma_h^\theta} n_{\Gamma_h^\theta}^T)(\nabla_{\Gamma_h^\theta} e_x^\theta)^T) A^\theta, \tag{3.17}$$

where $A^\theta = \nabla_{\Gamma_h^\theta} n_{\Gamma_h^\theta}$ denotes the piecewisely defined Weingarten matrix. By taking trace, applying $|\mathrm{tr}(AB)| \le \|A\|_F \|B\|_F$ and inverse inequality, we obtain

$$|\partial_\theta^\bullet H_{\Gamma_h^\theta}| \lesssim h^{-1} \|\nabla_{\Gamma_h^\theta} e_x^\theta\|_{L^\infty(\Gamma_h^\theta)} + \|A^\theta\|_F. \tag{3.18}$$

where $\|\cdot\|_F$ denotes the Frobenius norm. Furthermore, we have

$$\frac{d}{d\theta}\|A^\theta\|_F \le \|\partial_\theta^\bullet A^\theta\|_F \le \sum_{i=1}^{d} \|\nabla^2_{\Gamma_h^\theta} e^\theta_{xi}\|_F + 3\|A^\theta\|_F \|\nabla_{\Gamma_h^\theta} e^\theta_x\|_F$$
$$\lesssim h^{-1}\|\nabla_{\Gamma_h^\theta} e^\theta_x\|_{L^\infty(\Gamma_h^\theta)} + \|A^\theta\|_F.$$

Using Gronwall's inequality, and boundedness of $\|A^*\|_F$ from [17, Prop. 2.3] yields

$$\|A^\theta\|_F \lesssim \|A^*\|_F + h^{-1} \sup_{s\in[0,\theta]} \|\nabla_{\Gamma_h^s} e^s_x\|_{L^\infty(\Gamma_h^s)}$$
$$\lesssim \|A^*\|_F + h^{-1}\|\nabla_{\Gamma_h^*} e^0_x\|_{L^\infty(\Gamma_h^*)} \lesssim 1 + h^{-1}\|\nabla_{\Gamma_h^*} e^0_x\|_{L^\infty(\Gamma_h^*)}. \tag{3.19}$$

Then (3.14) is proved by combining (3.18)–(3.19) and integration over $[0,\theta]$.

Let E^θ be the edge that joins two adjacent elements $K^\theta_\pm$ on Γ_h^θ. According to (2.9), we obtain $\partial_\theta^\bullet n^\theta_\pm = -(\nabla_{\Gamma_h^\theta} e^\theta_x|_{K^\theta_\pm}) n^\theta_\pm$. Then

$$\partial_\theta^\bullet |n^\theta_+ - n^\theta_-|^2 = 2(n^\theta_+ - n^\theta_-, \partial_\theta^\bullet(n^\theta_+ - n^\theta_-)) \lesssim |n^\theta_+ - n^\theta_-| \|\nabla_{\Gamma_h^\theta} e^\theta_x\|_{L^\infty(\Gamma_h^\theta)}.$$

By using relation (2.5), we obtain the pointwise estimation

$$\partial_\theta^\bullet |[\mu]_{E^\theta}| = \partial_\theta^\bullet |n^\theta_+ - n^\theta_-| \lesssim \|\nabla_{\Gamma_h^*} e^0_x\|_{L^\infty(\Gamma_h^*)}. \tag{3.20}$$

By [17, Prop. 2.3], $\|[\mu]\|_{L^\infty(E^*)} \le \|n_+ - n^\ell_\Gamma\|_{L^\infty(K^*_+)} + \|n_- - n^\ell_\Gamma\|_{L^\infty(K^*_-)} \lesssim h^k$. Integrating (3.20) over $[0,\theta]$ yields

$$\|[\mu]\|_{L^\infty(E^\theta)} \lesssim \|[\mu]\|_{L^\infty(E^*)} + \|\nabla_{\Gamma_h^*} e^0_x\|_{L^\infty(\Gamma_h^*)} \lesssim h^k + \|\nabla_{\Gamma_h^*} e^0_x\|_{L^\infty(\Gamma_h^*)}. \tag{3.21}$$

□

3.3. Stability estimates. In this section, we present stability analysis for (3.8) under the following assumption.

Assumption 3.1. *There exists $t^* \ge 0$ such that for $t \in [0, t^*]$,*

$$\|e^0_x\|_{W^{1,\infty}(\Gamma_h^*)} \le h^{(k-1)/2}, \quad \|e^0_v\|_{W^{1,\infty}(\Gamma_h^*)} \le h^{(k-1)/2}, \tag{3.22a}$$
$$\|e^0_n\|_{W^{1,\infty}(\Gamma_h^*)} \le h^{(k-1)/2}, \quad \|e^0_n\|_{L^\infty(\Gamma_h^*)} \le h^{(k+1)/2}, \tag{3.22b}$$
$$\|e^0_p\|_{L^\infty(\Gamma_h^*)} \le h^{(k-1)/2}, \quad \|e^0_q\|_{L^\infty(\Gamma_h^*)} \le h^{(k-1)/2}. \tag{3.22c}$$

At the end of this section we shall prove that Assumption 3.1 holds for $t^* = T$ (when h is smaller than some constant).

The estimates for the transport term in (3.8c)–(3.8d) are presented in the following proposition, where the jump terms of conormals are estimated using Lemma 3.2.

Proposition 3.3 (Perturbation of the transport equation). *Let $k \ge 2$ and $z_h^{*,0}$, $v_h^{*,0}$ be uniformly bounded in $W^{1,\infty}(\Gamma_h[\mathbf{x}^*])$. Suppose that condition* (3.9) *and Assumption 3.1 hold true. Then we obtain*

$$\mathbf{e}_\mathbf{z}^T(\mathbf{E}(\mathbf{x},\mathbf{v})\mathbf{z} - \mathbf{E}(\mathbf{x}^*,\mathbf{v}^*)\mathbf{z}^*) \lesssim \|\mathbf{e}_\mathbf{x}\|^2_{\mathbf{K}^*} + \|\mathbf{e}_\mathbf{v}\|^2_{\mathbf{M}^*} + \|\mathbf{e}_\mathbf{z}\|^2_{\mathbf{M}^*}. \tag{3.23}$$

The proof of Proposition 3.3 relies on several lemmas established in the literature. For detailed proofs, refer to Proposition 2.7 in [17] and (A.4) in [30]. The only difference is the numerical suface Γ_h and it can be easily addressed using the norm equivalence (3.10) under assumption 3.1. Therefore, we omit their proof here.

Lemma 3.4. *Let I_{Γ_h} denote the interpolation into $S_h[\mathbf{x}]$. Under Assumption 3.1, the interpolated function $I_{\Gamma_h} u$ has the following error bound:*

$$\|u - I_{\Gamma_h} u\|_{L^\infty(\Gamma_h)} + h\|u - I_{\Gamma_h} u\|_{H^1(\Gamma_h)} \lesssim h^2. \tag{3.24}$$

Lemma 3.5. *Under Assumption 3.1, for* w_1, $w_2 \in S_h[\mathbf{x}]$,

$$\|w_1w_2 - I_{\Gamma_h}(w_1w_2)\|_{L^2(\Gamma_h)} \lesssim h^2\|w_1\|_{H^1(\Gamma_h)}\|w_2\|_{W^{1,\infty}(\Gamma_h)}. \tag{3.25}$$

Proof. [Proof of Proposition 3.3] We introduce the following finite element functions on Γ_h^θ: $v_h^\theta = v_h^{*,\theta} + \theta e_v^\theta$ and $z_h^\theta = z_h^{*,\theta} + \theta e_z^\theta$. By definition in (2.23), we derive

$$\mathbf{e}_\mathbf{z}^T(\mathbf{E}(\mathbf{x},\mathbf{v})\mathbf{z} - \mathbf{E}(\mathbf{x}^*,\mathbf{v}^*)\mathbf{z}^*) = \int_0^1 \frac{\mathbf{d}}{\mathbf{d}\theta}\int_{\Gamma_h^\theta}((v_h^\theta - u)\cdot\nabla_{\Gamma_h^\theta})(z_h^{*,\theta} + \theta e_z^\theta)\cdot e_z^\theta \mathbf{d}\theta = I_1 + I_2.$$

For I_1, by the Leibniz rule, $\partial_\theta^\bullet u = (e_x^\theta\cdot\nabla)u$ and (2.4), we have

$$\begin{aligned}
I_1 &= \int_0^1 \frac{\mathbf{d}}{\mathbf{d}\theta}\int_{\Gamma_h^\theta}((v_h^\theta - u)\cdot\nabla_{\Gamma_h^\theta})z_h^{*,\theta}\cdot e_z^\theta\mathbf{d}\theta\\
&= \int_0^1\int_{\Gamma_h^\theta}((v_h^\theta - u)\cdot\nabla_{\Gamma_h^\theta})z_h^{*,\theta}\cdot e_z^\theta\nabla_{\Gamma_h^\theta}\cdot e_x^\theta\mathbf{d}\theta + \int_0^1\int_{\Gamma_h^\theta}((e_v^\theta - \partial_\theta^\bullet u)\cdot\nabla_{\Gamma_h^\theta})z_h^{*,\theta}\cdot e_z^\theta\mathbf{d}\theta\\
&\quad + \int_0^1\int_{\Gamma_h^\theta}\Big(\big(-(\nabla_{\Gamma_h^\theta}e_x^\theta)^T + \nabla_{\Gamma_h^\theta}e_x^\theta n_{\Gamma_h^\theta}n_{\Gamma_h^\theta}^T\big)(v_h^\theta - u)\cdot\nabla_{\Gamma_h^\theta}\Big)z_h^{*,\theta}\cdot e_z^\theta\mathbf{d}\theta\\
&\lesssim (\|\mathbf{e_x}\|_{\mathbf{K}^*} + \|\mathbf{e_v}\|_{\mathbf{M}^*})\|\mathbf{e_z}\|_{\mathbf{M}^*}.
\end{aligned}$$

For I_2, we apply (2.8) to transfer the surface gradient from e_z to $v_h - u$ and obtain

$$\begin{aligned}
&\int_0^1\frac{\mathbf{d}}{\mathbf{d}\theta}\theta\int_{\Gamma_h^\theta}((v_h^\theta - u)\cdot\nabla_{\Gamma_h^\theta})e_z^\theta\cdot e_z^\theta\mathbf{d}\theta = \int_{\Gamma_h}((v_h - u)\cdot\nabla_{\Gamma_h})e_z\cdot e_z\\
&= \frac{1}{2}\Big[\sum_{E_h\in\mathcal{E}_h}\int_{E_h}|e_z|^2(v_h-u)\cdot[\mu]_{E_h} + \int_{\Gamma_h}|e_z|^2\big[H_{\Gamma_h}(v_h-u)\cdot n_{\Gamma_h} - \nabla_{\Gamma_h}\cdot(v_h-u)\big]\Big]\\
&= \frac{1}{2}\sum_{i=1}^2 J_i.
\end{aligned}$$

Next, we prove the smallness of $\|(v_h-u)\cdot n_{\Gamma_h}\|_{L^\infty(\Gamma_h)}$ which is implied by (2.18b). We first apply the inverse inequality to the globally continuous piecewise polynomial function $(v_h - I_{\Gamma_h}u)\cdot n_h$ after employing the triangle inequality. Then we get

$$\begin{aligned}
\|(v_h-u)\cdot n_h\|_{L^\infty(\Gamma_h)} &\lesssim h^{-1}\|(v_h - I_{\Gamma_h}u)\cdot n_h\|_{L^2} + \|(u - I_{\Gamma_h}u)\cdot n_h\|_{L^\infty}\\
&\lesssim h^{-1}\|(v_h-u)\cdot n_h\|_{L^2} + h^{-1}\|(u-I_{\Gamma_h}u)\cdot n_h\|_{L^2} + \|(u-I_{\Gamma_h}u)\cdot n_h\|_{L^\infty}\\
&\lesssim h^{-1}\|(v_h-u)\cdot n_h\|_{L^2} + h\|n_h\|_{L^\infty(\Gamma_h)},
\end{aligned}\tag{3.26}$$

where the second line results from triangle inequality and the last line results from Lemma 3.4. For the first term in (3.26), we test $\chi_\kappa = I_{\Gamma_h}((v_h - I_{\Gamma_h}u)\cdot n_h)$ in (2.18b) and obtain

$$\|(v_h-u)\cdot n_h\|_{L^2(\Gamma_h)} \le \|(v_h-u)\cdot n_h - I_{\Gamma_h}\left((v_h - I_{\Gamma_h}u)\cdot n_h\right)\|_{L^2(\Gamma_h)}. \tag{3.27}$$

By using the superconvergence result in Lemma 3.5 after applying triangle inequality to (3.27), we obtain

$$\|(v_h-u)\cdot n_h\|_{L^2(\Gamma_h)} \lesssim \|(u-I_{\Gamma_h}u)\cdot n_h\|_{L^2(\Gamma_h)} + h^2\|v_h - I_{\Gamma_h}u\|_{H^1(\Gamma_h)}\|n_h\|_{W^{1,\infty}(\Gamma_h)}.$$

Combining the above results leads to

$$\|(v_h-u)\cdot n_h\|_{L^\infty(\Gamma_h)} \lesssim h\left(1 + \|e_v\|_{H^1(\Gamma_h)} + \|e_x\|_{L^\infty(\Gamma_h)}\right)(1 + \|e_n\|_{W^{1,\infty}(\Gamma_h)}).$$

The difference of n_h and n_{Γ_h} is estimated by inserting the normal vector of Γ_h^*,

$$\begin{aligned}\|n_h - n_{\Gamma_h}\|_{L^\infty(\Gamma_h)} &\le \|n_h^1 - n_h^{*,1}\|_{L^\infty(\Gamma_h)} + \|n_h^{*,1} - n_{\Gamma_h^*} \circ b_1^{-1}\|_{L^\infty(\Gamma_h)} \\ &\quad + \|n_{\Gamma_h^*} \circ b_1^{-1} - n_{\Gamma_h}\|_{L^\infty(\Gamma_h)} \\ &\lesssim \|e_n\|_{L^\infty(\Gamma_h)} + h^k + \|e_x\|_{W^{1,\infty}(\Gamma_h)}.\end{aligned}$$

For $k \ge 2$, Assumption 3.1 yields the boundedness of e_n, e_x and e_v in $W^{1,\infty}(\Gamma_h)$. By combining the above two estimates, we derive that

$$\|(v_h - u) \cdot n_{\Gamma_h}\|_{L^\infty(\Gamma_h)} \lesssim h + \|e_n\|_{L^\infty(\Gamma_h)} + \|e_x\|_{W^{1,\infty}(\Gamma_h)}. \tag{3.28}$$

Let E_h be the common edge of the two adjacent elements $K_\pm$. By (2.6), we get

$$\begin{aligned}\|(v_h - u) \cdot [\mu]_{E_h}\|_{L^\infty(E_h)} &\lesssim \|(v_h - u) \cdot (n_{K_+} + n_{K_-})\|_{L^\infty(E_h)} \|[\mu]\|_{L^\infty(E_h)} \\ &\lesssim (h + \|e_n\|_{L^\infty(\Gamma_h)} + \|e_x\|_{W^{1,\infty}(\Gamma_h)}) \|[\mu]\|_{L^\infty(E_h)},\end{aligned}$$

where the last inequality is from (3.28). By using the trace inequality, we obtain

$$\begin{aligned}J_1 &= \sum_{E_h \in \mathcal{E}_h} \int_{E_h} (e_z)^2 (v_h - u) \cdot [\mu]_{E_h} \\ &\le (h^k + \|\nabla_{\Gamma_h^*} e_x^0\|_{L^\infty(\Gamma_h^*)})(h + \|e_n\|_{L^\infty(\Gamma_h)} + \|e_x\|_{W^{1,\infty}(\Gamma_h)}) \sum_{E_h \in \mathcal{E}_h} \|e_z\|_{L^2(E_h)}^2 \\ &\lesssim h^{-1}(h^k + \|\nabla_{\Gamma_h^*} e_x^0\|_{L^\infty(\Gamma_h^*)})(h + \|e_n^0\|_{L^\infty(\Gamma_h^*)} + \|e_x^0\|_{W^{1,\infty}(\Gamma_h^*)}) \|\mathbf{e_z}\|_{\mathbf{M}^*}^2.\end{aligned}$$

The term J_2 can be estimated by using Lemma 3.2 and (3.28), i.e.,

$$\begin{aligned}J_2 &\lesssim \Big(\|H_{\Gamma_h}\|_{L^\infty(\Gamma_h)} \|(v_h - u) \cdot n_{\Gamma_h}\|_{L^\infty(\Gamma_h)} + \|\nabla_{\Gamma_h} \cdot (v_h - u)\|_{L^\infty(\Gamma_h)}\Big) \|\mathbf{e_z}\|_{\mathbf{M}^*}^2 \\ &\lesssim (1 + h^{-1}\|\nabla_{\Gamma_h^*} e_x^0\|_{L^\infty(\Gamma_h^*)})(h + \|e_n^0\|_{L^\infty(\Gamma_h^*)} + \|e_x^0\|_{W^{1,\infty}(\Gamma_h^*)}) \|\mathbf{e_z}\|_{\mathbf{M}^*}^2 \\ &\quad + (1 + \|e_v^0\|_{W^{1,\infty}(\Gamma_h^*)}) \|\mathbf{e_z}\|_{\mathbf{M}^*}^2.\end{aligned}$$

For $k \ge 2$, the estimates of I_1, J_1 and J_2 lead to $I_1 + I_2 \lesssim \|\mathbf{e_x}\|_{\mathbf{K}^*}^2 + \|\mathbf{e_v}\|_{\mathbf{M}^*}^2 + \|\mathbf{e_z}\|_{\mathbf{M}^*}^2$. This proves the result of Proposition 3.3. □

Lemma 3.6. *Under Assumption 3.1, the following result holds for $k \ge 2$:*

$$\mathbf{e_V}^T(\mathbf{KV}(\mathbf{x}, \mathbf{n}) - \mathbf{K}^*\mathbf{V}(\mathbf{x}^*, \mathbf{n}^*)) \lesssim (\|\mathbf{e_n}\|_{\mathbf{K}^*} + \|\mathbf{e_x}\|_{\mathbf{K}^*}) \|\mathbf{e_V}\|_{\mathbf{K}^*}. \tag{3.29}$$

Proof. Since $\mathbf{K} = \mathbf{M} + \mathbf{A}$, we only need to prove the following result which corresponds to $\mathbf{A}$ (the part corresponding to $\mathbf{M}$ is simpler and omitted):

$$\mathbf{e_V}^T(\mathbf{AV}(\mathbf{x}, \mathbf{n}) - \mathbf{A}^*\mathbf{V}(\mathbf{x}^*, \mathbf{n}^*)) \lesssim (\|\mathbf{e_n}\|_{\mathbf{K}^*} + \|\mathbf{e_x}\|_{\mathbf{K}^*}) \|\mathbf{e_V}\|_{\mathbf{A}^*}. \tag{3.30}$$

Let us abbreviate $\mathbf{V}(\mathbf{x}^*, \mathbf{n}^*)$ (see (2.27)) as $\mathbf{V}^*$. Note that $\mathbf{V}^*$ collects the nodal values of $P_{\Gamma_h^*}(u \cdot n_h^*) \in S_h[\mathbf{x}^*]$, where $P_{\Gamma_h^*}$ denotes the L^2 projection onto $S_h[\mathbf{x}^*]$. Thus, we derive

$$\begin{aligned}\mathbf{e_V}^T(\mathbf{AV} - \mathbf{A}^*\mathbf{V}^*) &= \int_0^1 \frac{d}{d\theta} \int_{\Gamma_h^\theta} \nabla_{\Gamma_h^\theta} P_{\Gamma_h^\theta}(u \cdot n_h^\theta) \cdot \nabla_{\Gamma_h^\theta} e_V^\theta \\ &= \int_0^1 \int_{\Gamma_h^\theta} D_{\Gamma_h^\theta} e_x^\theta \nabla_{\Gamma_h^\theta} P_{\Gamma_h^\theta}(u \cdot n_h^\theta) \cdot \nabla_{\Gamma_h^\theta} e_V^\theta + \nabla_{\Gamma_h^\theta} \partial_\theta^\bullet P_{\Gamma_h^\theta}(u \cdot n_h^\theta) \cdot \nabla_{\Gamma_h^\theta} e_V^\theta,\end{aligned}$$

where $D_{\Gamma_h^\theta} e_x^\theta = \mathrm{tr}(E^\theta) I_d - (E^\theta + (E^\theta)^T)$ and $E^\theta = \nabla_{\Gamma_h^\theta} e_x^\theta$. According to [30, (3.21)], the material derivative of L^2 projection has the explicit formula,

$$\partial_\theta^\bullet P_{\Gamma_h^\theta}(u \cdot n_h^\theta) = P_{\Gamma_h^\theta}((e_x^\theta \cdot \nabla) u \cdot n_h^\theta + u \cdot e_n^\theta) + P_{\Gamma_h^\theta}\left[(I - P_{\Gamma_h^\theta})(u \cdot n_h^\theta) \nabla_{\Gamma_h^\theta} \cdot e_x^\theta\right].$$

For the simplicity of notation, we denote

$$K_0 = \nabla_{\Gamma_h^\theta} P_{\Gamma_h^\theta}(u \cdot n_h^\theta), \quad K_1 = P_{\Gamma_h^\theta}(u \cdot e_n^\theta),$$
$$K_2 = P_{\Gamma_h^\theta}(e_x^\theta \cdot \nabla) u \cdot n_h^\theta, \quad K_3 = P_{\Gamma_h^\theta}\big[(I - P_{\Gamma_h^\theta})(u \cdot n_h^\theta)\nabla_{\Gamma_h^\theta} \cdot e_x^\theta\big],$$

so that the expression of $\mathbf{e}_{\mathbf{V}}^T(\mathbf{AV} - \mathbf{A}^*\mathbf{V}^*)$ derived above can be written as

$$\mathbf{e}_{\mathbf{V}}^T(\mathbf{AV} - \mathbf{A}^*\mathbf{V}^*) = \int_{\Gamma_h^\theta} (D_{\Gamma_h^\theta} e_x^\theta) K_0 \cdot \nabla_{\Gamma_h^\theta} e_V^\theta + \nabla_{\Gamma_h^\theta}(K_1 + K_2 + K_3) \cdot \nabla_{\Gamma_h^\theta} e_V^\theta.$$

By inverse inequality and Lemma 3.5, we obtain

$$\begin{aligned}\|\nabla_{\Gamma_h^\theta} K_1\|_{L^2} &\le \|\nabla_{\Gamma_h^\theta} P_{\Gamma_h^\theta}((I - I_{\Gamma_h^\theta})u \cdot e_n^\theta)\|_{L^2} + \|\nabla_{\Gamma_h^\theta}(I - P_{\Gamma_h^\theta})(I_{\Gamma_h^\theta} u \cdot e_n^\theta)\|_{L^2} \\ &\quad + \|\nabla_{\Gamma_h^\theta}(I_{\Gamma_h^\theta} u \cdot e_n^\theta)\|_{L^2} \\ &\lesssim h^{-1}\|(I - I_{\Gamma_h^\theta})u \cdot e_n^\theta\|_{L^2} + h\|I_{\Gamma_h^\theta} u\|_{W^{1,\infty}}\|e_n^\theta\|_{H^1} + \|e_n^\theta\|_{H^1}.\end{aligned}$$

Likewise, we have

$$\begin{aligned}\|\nabla_{\Gamma_h^\theta} K_3\|_{L^2} &\lesssim h^{-1}\|(I - P_{\Gamma_h^\theta})(u \cdot n_h^\theta)\nabla_{\Gamma_h^\theta} \cdot e_x^\theta\|_{L^2} \\ &\lesssim h^{-1}\left(\|(I - P_{\Gamma_h^\theta})(u \cdot n_h^{*,\theta})\|_{L^\infty}\|\nabla_{\Gamma_h^\theta} \cdot e_x^\theta\|_{L^2} + \|(I - I_h^\theta)(u \cdot e_n^\theta)\|_{L^2}\right) \\ &\lesssim \|\mathbf{e_n}\|_{\mathbf{K}^*} + \|\mathbf{e_x}\|_{\mathbf{K}^*}.\end{aligned}$$

The other terms have no essential differences. Therefore, (3.30) is proved. □

Proposition 3.7 (Stability estimates). *Suppose that $k \ge 2$ and Assumption 3.1 holds. There exists $h_0 > 0$ such that for $h \le h_0$, the errors in* (3.8a)– (3.8e) *satisfy the following stability results*

$$\|\mathbf{e_x}(t)\|_{\mathbf{K}^*}^2 \lesssim \int_0^t \|\mathbf{e_v}\|_{\mathbf{K}^*}^2 + \|\mathbf{e_x}\|_{\mathbf{K}^*}^2 \,\mathrm{d}s, \tag{3.31}$$

$$\|\mathbf{e_v}(t)\|_{\mathbf{K}^*} \lesssim \|\mathbf{e_x}(t)\|_{\mathbf{K}^*} + \|\mathbf{e_n}(t)\|_{\mathbf{K}^*} + \|\mathbf{d_v}(t)\|_{\mathbf{M}^*} + \|\mathbf{d}_{\boldsymbol{\kappa}}(t)\|_{\mathbf{M}^*}, \tag{3.32}$$

$$\|\mathbf{e_p}(t)\|_{\mathbf{M}^*}^2 \lesssim \|\mathbf{e_p}(0)\|_{\mathbf{M}^*}^2 + \int_0^t \|\mathbf{e_x}\|_{\mathbf{K}^*}^2 + \|\mathbf{e_v}\|_{\mathbf{M}^*}^2 + \|\mathbf{e_p}\|_{\mathbf{M}^*}^2 + \|\mathbf{e_q}\|_{\mathbf{M}^*}^2 + \|\mathbf{d_p}\|_{\mathbf{M}^*}^2 \mathbf{d}s, \tag{3.33}$$

$$\|\mathbf{e_q}(t)\|_{\mathbf{M}^*}^2 \lesssim \|\mathbf{e_q}(0)\|_{\mathbf{M}^*}^2 + \int_0^t \|\mathbf{e_x}\|_{\mathbf{K}^*}^2 + \|\mathbf{e_v}\|_{\mathbf{K}^*}^2 + \|\mathbf{e_p}\|_{\mathbf{M}^*}^2 + \|\mathbf{e_q}\|_{\mathbf{M}^*}^2 + \|\mathbf{d_q}\|_{\mathbf{M}^*}^2 \mathbf{d}s, \tag{3.34}$$

$$\|\mathbf{e_n}\|_{\mathbf{K}^*}^2 \lesssim \|\mathbf{e_x}\|_{\mathbf{A}^*}^2 + \|\mathbf{e_p}\|_{\mathbf{M}^*}^2 + \|\mathbf{e_q}\|_{\mathbf{M}^*}^2 + \|\mathbf{d_n}\|_*^2. \tag{3.35}$$

Proof. The proof consists of three parts that correspond to the velocity equation (3.8a)-(3.8b), the evolving normal and Weingarten matrix (3.8c)–(3.8d) and the recovered normal part (3.8e) respectively.

Compared with [30, (3.10b)–(3.10c)], the velocity part has the same form after replacing the normal velocity from the mean curvature $\mathbf{H}$ in [30] to $\mathbf{V}$. Then we deduce that for $k \ge 2$ and $t \in [0, t^*]$,

$$\|\mathbf{e_v}(t)\|_{\mathbf{K}^*} \lesssim \|\mathbf{e_x}(t)\|_{\mathbf{K}^*} + \|\mathbf{e_n}(t)\|_{\mathbf{K}^*} + \|\mathbf{e_V}(t)\|_{\mathbf{K}^*} + \|\mathbf{d_v}(t)\|_{\mathbf{M}^*} + \|\mathbf{d}_{\boldsymbol{\kappa}}(t)\|_{\mathbf{M}^*}. \tag{3.36}$$

According to (3.29) in the preceding lemma,

$$\begin{aligned}\|\mathbf{e_V}\|_{\mathbf{K}^*}^2 &\lesssim \|\mathbf{e_V}\|_{\mathbf{K}}^2 = \mathbf{e}_{\mathbf{V}}^T(\mathbf{KV} - \mathbf{K}^*\mathbf{V}^*) + \mathbf{e}_{\mathbf{V}}^T(\mathbf{K}^* - \mathbf{K})\mathbf{V}^* \\ &\lesssim (\|\mathbf{e_n}\|_{\mathbf{K}^*} + \|\mathbf{e_x}\|_{\mathbf{K}^*})\|\mathbf{e_V}\|_{\mathbf{K}^*},\end{aligned} \tag{3.37}$$

Substituting the estimation of $\|\mathbf{e_V}\|_{\mathbf{K}^*}$ into (3.36) yields (3.32).

Inequalities (3.33)–(3.34) are proved by employing the energy estimation to (3.8c) and (3.8d) with test functions $\mathbf{e_p}$ and $\mathbf{e_q}$ respectively and using the bilinear error estimate (3.23). Here we only present a detailed proof of (3.34). A similar proof can be applied to (3.8c) by treating a simpler nonlinear term. Testing (3.8d) with $\mathbf{e_q}$, we derive

$$\mathbf{e_q}^T\mathbf{M}\dot{\mathbf{e}}_\mathbf{q} = \mathbf{e_q}^T(\mathbf{E}\mathbf{q} - \mathbf{E}^*\mathbf{q}^*) + \mathbf{e_q}^T(\mathbf{M}^* - \mathbf{M})\dot{\mathbf{q}}^* + \mathbf{e_q}^T(\mathbf{g} - \mathbf{g}^*) - \mathbf{e_q}^T\mathbf{M}^*\mathbf{d_q}. \tag{3.38}$$

By using Leibniz rule, [36, (7.11)] and norm equivalence (3.10), the first term can be estimated as follows,

$$\mathbf{e_q}^T\mathbf{M}\dot{\mathbf{e}}_\mathbf{q} = -\frac{1}{2}\mathbf{e_q}^T\frac{\mathbf{d}}{\mathbf{d}t}\mathbf{M}\mathbf{e_q} + \frac{1}{2}\frac{\mathbf{d}}{\mathbf{d}t}\left(\mathbf{e_q}^T\mathbf{M}\mathbf{e_q}\right) \geq -c\|\mathbf{e_q}\|^2_{\mathbf{M}^*} + \frac{1}{2}\frac{\mathbf{d}}{\mathbf{d}t}\|\mathbf{e_q}\|^2_{\mathbf{M}}.$$

Applying (3.23) and (3.11), we derive

$$\mathbf{e_q}^T(\mathbf{E}\mathbf{q} - \mathbf{E}^*\mathbf{q}^*) + \mathbf{e_q}^T(\mathbf{M}^* - \mathbf{M})\dot{\mathbf{q}}^* \lesssim \|\mathbf{e_x}\|^2_{\mathbf{K}^*} + \|\mathbf{e_v}\|^2_{\mathbf{M}^*} + \|\mathbf{e_q}\|^2_{\mathbf{M}^*}. \tag{3.39}$$

By Newton-Leibniz formula, the third term can be rewritten as an integral,

$$\begin{aligned}\mathbf{e_q}^T(\mathbf{g} - \mathbf{g}^*) &= \int_0^1 \frac{\mathbf{d}}{\mathbf{d}\theta}\int_{\Gamma_h^\theta} g(U, p_{\Gamma_h^\theta}, q_{\Gamma_h^\theta}, v_{\Gamma_h^\theta}, \nabla_{\Gamma_h^\theta} v_{\Gamma_h^\theta}) : e_q^\theta d\theta \\ &= \int_0^1 \int_{\Gamma_h^\theta} (\partial_\theta^\bullet g(U, p_{\Gamma_h^\theta}, q_{\Gamma_h^\theta}, v_{\Gamma_h^\theta}, \nabla_{\Gamma_h^\theta} v_{\Gamma_h^\theta}) + g\nabla_{\Gamma_h^\theta}\cdot e_x^\theta) : e_q^\theta d\theta,\end{aligned}$$

where $p_{\Gamma_h^\theta}$, $q_{\Gamma_h^\theta}$ and $v_{\Gamma_h^\theta}$ are finite element functions in $S_h[\mathbf{x}^\theta]$ corresponding to $\mathbf{p}^*+\theta\mathbf{e_p}$, $\mathbf{q}^* + \theta\mathbf{e_q}$ and $\mathbf{v}^* + \theta\mathbf{e_v}$, respectively. Recalling the Assumption 3.1 and the smoothness of u, we deduce that $p_{\Gamma_h^\theta}$, $q_{\Gamma_h^\theta}$, $U|_{\Gamma_h^\theta}$ and $\nabla U|_{\Gamma_h^\theta}$ are bounded in $L^\infty(\Gamma_h^\theta)$, $v_{\Gamma_h^\theta}$ is bounded in $W^{1,\infty}(\Gamma_h^\theta)$. Then the smoothness (local Lipschitz) of g (see (2.15)) yields $\|g(U, p_{\Gamma_h^\theta}, q_{\Gamma_h^\theta}, v_{\Gamma_h^\theta}, \nabla_{\Gamma_h^\theta} v_{\Gamma_h^\theta})\|_{L^\infty(\Gamma_h^\theta)} \leq C$ and $\|\partial_i g(U, p_{\Gamma_h^\theta}, q_{\Gamma_h^\theta}, v_{\Gamma_h^\theta}, \nabla_{\Gamma_h^\theta} v_{\Gamma_h^\theta})\|_{L^\infty(\Gamma_h^\theta)} \leq C$ for $i = 1, \cdots, 5$. This, together with

$$\begin{aligned}&\partial_\theta^\bullet U = (e_x^\theta\cdot\nabla)U, \quad \partial_\theta^\bullet p_{\Gamma_h^\theta} = e_p^\theta, \quad \partial_\theta^\bullet q_{\Gamma_h^\theta} = e_q^\theta, \quad \partial_\theta^\bullet v_{\Gamma_h^\theta} = e_v^\theta, \\ &\partial_\theta^\bullet \nabla_{\Gamma_h^\theta} v_{\Gamma_h^\theta} = \nabla_{\Gamma_h^\theta} e_v^\theta - (\nabla_{\Gamma_h^\theta} e_x^\theta - n_{\Gamma_h^\theta} n_{\Gamma_h^\theta}^T(\nabla_{\Gamma_h^\theta} e_x^\theta)^T)\nabla_{\Gamma_h^\theta} v_{\Gamma_h^\theta},\end{aligned}$$

implies that

$$\mathbf{e_q}^T(\mathbf{g} - \mathbf{g}^*) \lesssim \|\mathbf{e_q}\|_{\mathbf{M}^*}\left(\|\mathbf{e_x}\|_{\mathbf{K}^*} + \|\mathbf{e_p}\|_{\mathbf{M}^*} + \|\mathbf{e_q}\|_{\mathbf{M}^*} + \|\mathbf{e_v}\|_{\mathbf{K}^*}\right).$$

Thus, (3.34) is obtained by integrating the following inequality from 0 to t,

$$\frac{\mathbf{d}}{\mathbf{d}t}\|\mathbf{e_q}\|^2_{\mathbf{M}^*} \lesssim \|\mathbf{e_q}\|^2_{\mathbf{M}^*} + \|\mathbf{d_q}\|^2_{\mathbf{M}^*} + \|\mathbf{e_x}\|^2_{\mathbf{K}^*} + \|\mathbf{e_v}\|^2_{\mathbf{K}^*} + \|\mathbf{e_p}\|^2_{\mathbf{M}^*}.$$

To prove (3.35), we test (3.8e) with $\mathbf{e_n}$ and obtain

$$\mathbf{e_n}^T\mathbf{K}\mathbf{e_n} = \mathbf{e_n}^T\mathbf{M}\mathbf{e_p} + \mathbf{e_n}^T(\mathbf{K}^* - \mathbf{K})\mathbf{n}^* - \mathbf{e_n}^T(\mathbf{M}^* - \mathbf{M})\mathbf{p}^* + \mathbf{e_n}^T(\mathbf{F} - \mathbf{F}^*) - \mathbf{e_n}^T\mathbf{M}^*\mathbf{d_n}, \tag{3.40}$$

where $\mathbf{F}$ and $\mathbf{F}^*$ are abbreviations for $\mathbf{F}(\mathbf{x}, \mathbf{q})$ and $\mathbf{F}(\mathbf{x}^*, \mathbf{q}^*)$. Since $\|n_h^*\|_{W^{1,\infty}(\Gamma_h^*)}$ and $\|p_h^*\|_{L^\infty(\Gamma_h^*)}$ are bounded, using the bilinear estimations (3.11)-(3.12), we derive

$$\mathbf{e_n}^T(\mathbf{K}^* - \mathbf{K})\mathbf{n}^* - \mathbf{e_n}^T(\mathbf{M}^* - \mathbf{M})\mathbf{p}^* \lesssim \|\mathbf{e_n}\|_{\mathbf{K}^*}\|\mathbf{e_x}\|_{\mathbf{A}^*}.$$

According to (2.25), we obtain

$$\mathbf{e_n}^T(\mathbf{F} - \mathbf{F}^*) = \int_0^1 \frac{\mathbf{d}}{\mathbf{d}\theta}\int_{\Gamma_h^\theta} q_{\Gamma_h^\theta} : \nabla_{\Gamma_h^\theta} e_n^\theta \mathbf{d}\theta$$

$$
\begin{aligned}
&= \int_0^1 \int_{\Gamma_h^\theta} e_q^\theta : \nabla_{\Gamma_h^\theta} e_n^\theta \mathrm{d}\theta + \int_0^1 \int_{\Gamma_h^\theta} q_{\Gamma_h^\theta} : \nabla_{\Gamma_h^\theta} e_n^\theta \nabla_{\Gamma_h^\theta} \cdot e_x^\theta \mathrm{d}\theta \\
&\quad + \int_0^1 \int_{\Gamma_h^\theta} q_{\Gamma_h^\theta} : (-(\nabla_{\Gamma_h^\theta} e_x^\theta - n_{\Gamma_h^\theta} n_{\Gamma_h^\theta}^T (\nabla_{\Gamma_h^\theta} e_x^\theta)^T)) \nabla_{\Gamma_h^\theta} e_n^\theta \mathrm{d}\theta \\
&\lesssim \|\mathbf{e_n}\|_{\mathbf{K}^*} (\|\mathbf{e_q}\|_{\mathbf{M}^*} + \|\mathbf{e_x}\|_{\mathbf{A}^*}).
\end{aligned}
$$

By applying the norm equivalence (3.10) and Young's inequality, we obtain

$$
\begin{aligned}
\|\mathbf{e_n}\|_{\mathbf{K}^*}^2 \le C \mathbf{e_n}^T \mathbf{K} \mathbf{e_n} &\le C \|\mathbf{e_n}\|_{\mathbf{K}^*} (\|\mathbf{e_x}\|_{\mathbf{A}^*} + \|\mathbf{e_p}\|_{\mathbf{M}^*} + \|\mathbf{e_q}\|_{\mathbf{M}^*} + \|\mathbf{d_n}\|_*) \\
&\le \frac{1}{2} \|\mathbf{e_n}\|_{\mathbf{K}^*}^2 + c(\|\mathbf{e_x}\|_{\mathbf{A}^*}^2 + \|\mathbf{e_p}\|_{\mathbf{M}^*}^2 + \|\mathbf{e_q}\|_{\mathbf{M}^*}^2 + \|\mathbf{d_n}\|_*^2).
\end{aligned}
$$

By absorption, we finish the proof of (3.35). ∎

3.4. Error estimates. The following lemma of consistency estimates can be shown by using the geometric perturbation errors between bilinear forms on the continuous surface and the interpolated surface. In particular, the estimation of $\|\mathbf{d_v}\|_{\mathbf{M}^*}$ and $\|\mathbf{d}_{\boldsymbol{\kappa}}\|_{\mathbf{M}^*}$ can be found in [30, Lemma 3.9], and the estimation of $\|\mathbf{d_n}\|_*$, $\|\mathbf{d_p}\|_{\mathbf{M}^*}$ and $\|\mathbf{d_q}\|_{\mathbf{M}^*}$ is standard and therefore omitted.

Lemma 3.8 (Consistency estimates). *Under the conditions of Theorem 2.1, the consistency errors defined in* (3.3)–(3.7) *satisfy the following estimates:*

$$
\|\mathbf{d_v}\|_{\mathbf{M}^*} + \|\mathbf{d}_{\boldsymbol{\kappa}}\|_{\mathbf{M}^*} + \|\mathbf{d_n}\|_* + \|\mathbf{d_p}\|_{\mathbf{M}^*} + \|\mathbf{d_q}\|_{\mathbf{M}^*} \lesssim h^k. \tag{3.41}
$$

Since $\mathbf{x}(0)$, $\mathbf{p}(0)$, $\mathbf{q}(0)$ are chosen as Lagrange interpolations in the same way as $\mathbf{x}^*$, $\mathbf{p}^*$ and $\mathbf{q}^*$, we obtain $\mathbf{e_p} = 0$, $\mathbf{e_q} = 0$ and $\mathbf{e_x} = 0$. After solving $\mathbf{n}(0)$ and $\mathbf{v}(0)$ from (2.28f) and (2.28b)–(2.28c), according to (3.32), (3.35) and Lemma 3.8, the following bound can be satisfied for sufficiently small h,

$$
\|\mathbf{e_p}(0)\|_{\mathbf{M}^*} + \|\mathbf{e_q}(0)\|_{\mathbf{M}^*} + \|\mathbf{e_x}(0)\|_{\mathbf{K}^*} + \|\mathbf{e_n}(0)\|_{\mathbf{K}^*} + \|\mathbf{e_v}(0)\|_{\mathbf{K}^*} \lesssim h^k. \tag{3.42}
$$

By inverse inequalities and continuity, there exists $t^* > 0$ such that the Assumption 3.1 holds for $t \in [0, t^*]$. Then for $k \ge 2$, there exists $h_0 > 0$ such that for $h \le h_0$, (3.31)–(3.32) and Lemma 3.7 hold for $t \in [0, t^*]$. Without loss of generality, we can take $t^* \in [0, T]$ to be the supreme value such that Assumption 3.1 holds. By substituting estimations of $\mathbf{e_v}$ and $\mathbf{e_n}$ into (3.31)–(3.32), we derive the following Grönwall type inequality,

$$
\begin{aligned}
&\|\mathbf{e_x}(t)\|_{\mathbf{K}^*}^2 + \|\mathbf{e_p}(t)\|_{\mathbf{M}^*}^2 + \|\mathbf{e_q}(t)\|_{\mathbf{M}^*}^2 \\
&\lesssim \int_0^t \|\mathbf{e_x}(s)\|_{\mathbf{K}^*}^2 + \|\mathbf{e_p}(s)\|_{\mathbf{M}^*}^2 + \|\mathbf{e_q}(s)\|_{\mathbf{M}^*}^2 \mathrm{d}s \\
&+ \int_0^t \|\mathbf{d_v}(s)\|_{\mathbf{M}^*}^2 + \|\mathbf{d}_{\boldsymbol{\kappa}}(s)\|_{\mathbf{M}^*}^2 + \|\mathbf{d_n}(s)\|_*^2 + \|\mathbf{d_p}(s)\|_{\mathbf{M}^*}^2 + \|\mathbf{d_q}(s)\|_{\mathbf{M}^*}^2 \mathrm{d}s.
\end{aligned}
$$

Using the consistency error bound in Lemma 3.8, we obtain by Grönwall's inequality that

$$
\|\mathbf{e_x}(t)\|_{\mathbf{K}^*}^2 + \|\mathbf{e_p}(t)\|_{\mathbf{M}^*}^2 + \|\mathbf{e_q}(t)\|_{\mathbf{M}^*}^2 \lesssim h^k.
$$

Consequently, by (3.32) and (3.35), we obtain

$$
\|\mathbf{e_v}(t)\|_{\mathbf{K}^*} + \|\mathbf{e_n}(t)\|_{\mathbf{K}^*} \lesssim h^k.
$$

By the continuity of semidiscrete finite element solutions in time, the above estimate still holds for $[0, t_* + \delta]$. By inverse inequality, there exists $h_0 > 0$ such that for $h \le h_0$,

the Assumption 3.1 holds for $[0, t_* + \delta]$. Hence we have $t_* = T$ and (3.42) holds for all $t \in [0, T]$. Thus, the proof of Theorem 2.1 can be completed by combining the error estimates of the Ritz projection and Lagrange interpolation of the projected solutions introduced in Section 3.1.

4. Numerical examples. In this section, we present numerical examples to support the theoretical results obtained in Theorem 2.1 by demonstrating the convergence of numerical approximations and the improvement of mesh quality by the proposed method. In addition, we present an example to show the capability of the proposed artificial tangential velocity in improving the effectiveness of the arbitrary Lagrangian–Eulerian method for solving PDEs on a domain with moving boundary. The evolving surface FEMs in the bulk and the surface are both implemented by the open sourced high performance Python package: NGsolve; see https://ngsolve.org.

Example 4.1 (Convergence of numerical approximations). We test the errors and convergence rates of the proposed method by considering the evolution of a hypersurface $S(t) \subset \mathbb{R}^d$ with $d = 2, 3$ under the velocity field

$$u(x, t) = x(1 - |x|), \tag{4.1}$$

with $S(0) = \{x \in \mathbb{R}^d : |x| = 1/2\}$ being the circle/sphere of radius $1/2$. In this case, the sphere $S(t)$ is a circle/sphere centered at the origin with radius $r = r(t)$ which satisfies the differential equation $dr/dt = r(1 - r)$, and the modified velocity v determined by (1.3b)–(1.3c) coincides with the original velocity u on $S(t)$. The solution with initial condition $r(0) = 1/2$ is given by $r(t) = 1/(1 + \exp(-t))$.

We approximate the surface evolution by the proposed method with a semi-implicit k-step backward differentiation formula (with k being the same of the degree of finite elements in space), with a sufficiently small time stepsize so that the errors from time discretization are negligibly small in observing the convergence rates of the spatial discretizations. The H^1 errors of position, velocity and normal vector, i.e., $\|\mathbf{e_x}\|_{\mathbf{K}^*}$, $\|\mathbf{e_v}\|_{\mathbf{K}^*}$ and $\|\mathbf{e_n}\|_{\mathbf{K}^*}$ and the L^2 norm of errors in $\mathbf{Q}$, i.e., $\|\mathbf{e_Q}\|^2_{\mathbf{M}^*} = \|\mathbf{e_p}\|^2_{\mathbf{M}^*} + \|\mathbf{e_q}\|^2_{\mathbf{M}^*}$, are presented in Figure 4.1. For both curves in 2D and surfaces in 3D, we observe kth-order convergence with respect to the mesh size h. This is consistent with the theoretical result proved in Theorem 2.1.

Example 4.2 (Improvement of mesh quality). We consider the evolution of a curve $\Gamma(t) \subset \mathbb{R}^2$ under velocity field (4.1), with initial condition

$$\Gamma(0) = \Big\{(x, y) \in \mathbb{R}^2 : \Big(x - \frac{1}{4}\Big)^2 + \Big(y - \frac{1}{4}\Big)^2 = \frac{1}{4}\Big\}. \tag{4.2}$$

The evolving curve is approximated by using the proposed method in (2.18) with finite elements of degree $k = 3$ and the semi-implicit Euler method in time discretization. The trajectories of the mesh points given by velocity field u and the proposed method are demonstrated in Figure 4.2 (b) and (c), respectively. Clearly, the proposed method effectively improves the mesh quality on the evolving curve.

Next, we consider an evolving surface $\Gamma(t) = \{(x, y, z) \in \mathbb{R}^3 : \varphi(x, y, z, t) = 1\}$ described by a level set function

$$\varphi(x, y, z, t) = \frac{x^2}{a^2(t)} + \frac{y^2}{a^2(t)} + G\Big(\frac{z^2}{L^2(t)}\Big).$$

with $G(s) = 200s(s - 199/200)$, $a(t) = 0.1 + 0.05\sin(2\pi t)$ and $L(t) = 1 + 0.2\sin(4\pi t)$. The surface evolves under the following velocity field:

$$u(x, y, z, t) = -\frac{\varphi_t \nabla\varphi}{|\nabla\varphi|^2}. \tag{4.3}$$

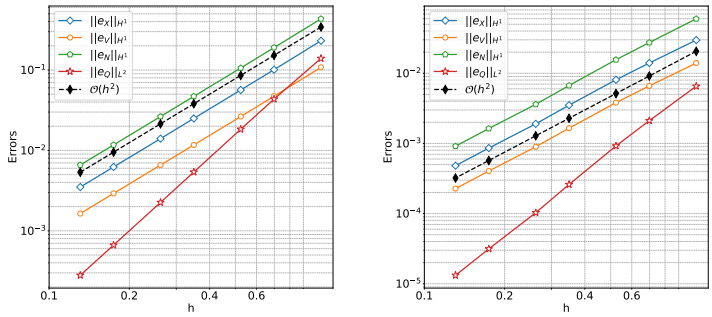

(a) Expansion of circles in 2D, k=2 (b) Expansion of spheres in 3D, k=2

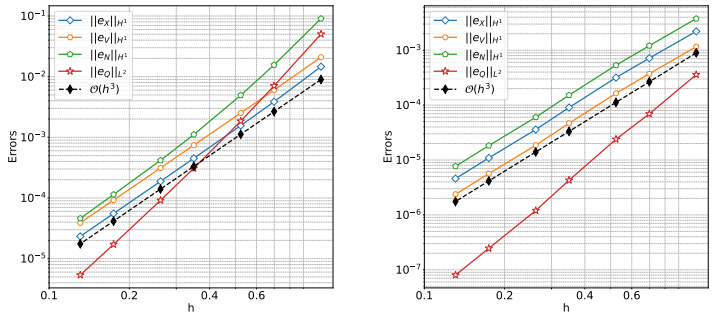

(c) Expansion of circles in 2D, k=3 (d) Expansion of spheres in 3D, k=3

Fig. 4.1. *Errors of numerical solutions at* $T = 1/8$ *(Example 4.1).*

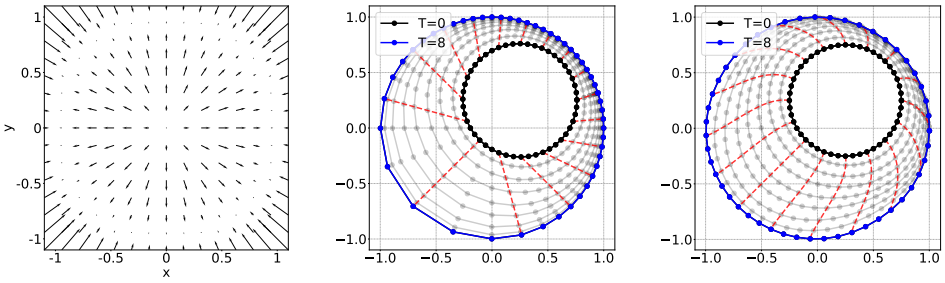

(a) The velocity field u (b) Trajectories under velocity u (c) Trajectories in our method

Fig. 4.2. *Evolution of a curve* $\Gamma(t)$ *under velocity field* u *(Example 4.2).*

This example is considered in [24] for illustrating the importance of using tangential motion to improve the mesh quality of a discrete surface.

Using the same initial mesh, we compare the performance of the proposed method with $k = 1$ and $k = 4$, the direct method, and Scheme (2.19) with finite elements of degree $k = 1$ and $k = 4$ in approximating the evolving surface at $T = 0.6$. Figure 4.3

shows the initial mesh and the approximate meshes at $T = 0.6$.

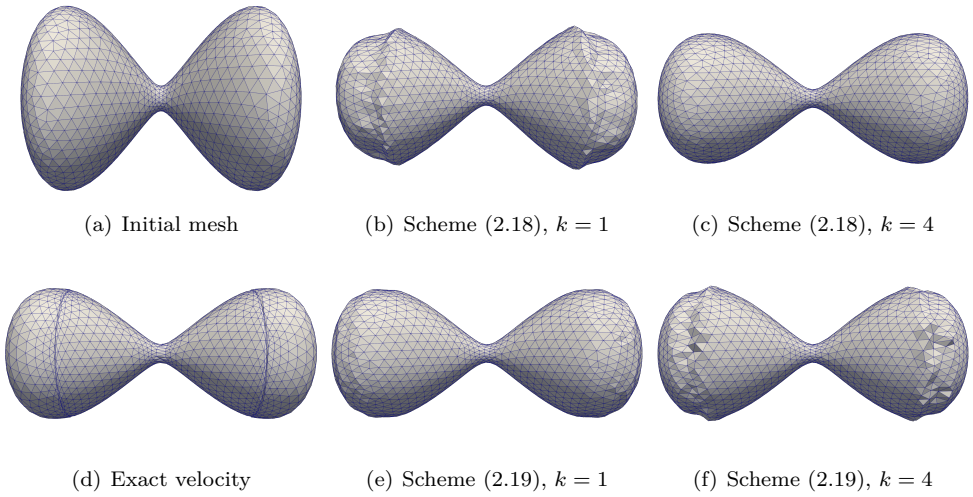

(a) Initial mesh (b) Scheme (2.18), $k = 1$ (c) Scheme (2.18), $k = 4$

(d) Exact velocity (e) Scheme (2.19), $k = 1$ (f) Scheme (2.19), $k = 4$

Fig. 4.3. *Evolving surface at $T = 0.6$ computed by the proposed method ($k = 1$ in (b) and $k = 4$ in (c)), the direct method (d) and Scheme* (2.19) *in Remark 2.1 ($k = 1$ in (e) and $k = 4$ in (f)) (Example 4.2).*

Compared to the clustered mesh obtained using the exact velocity field (i.e., Figure 4.3 (d)), the numerical results show that the proposed Scheme (2.18) with $k = 4$ improves the mesh quality while keeping accurate in approximating the shape of the surface, while the proposed Scheme (2.18) with $k = 1$ is inaccurate in approximating the shape of the surface. Scheme (2.19) with $k = 1$ also improves the mesh quality but with less accuracy, while Scheme (2.19) with $k = 4$ leads to worse results instead of higher accuracy.

The numerical results indicate that the proposed Scheme (2.18) with high-order finite elements can improve both mesh quality and accuracy in approximating the shape of the surface. It is also the only scheme among these that is proved convergent to the exact surface evolution.

Example 4.3 (Improvement of mesh quality). We consider the following velocity field:

$$u(x,t) = x(1-|x|^2) + \Big(1.2 - 0.2\frac{x_2}{|x|}\Big)(-x_2, x_1). \tag{4.4}$$

As visualized in Figure 4.4, the velocity field rotates anticlockwise. The evolutions of the curve $\Gamma(t)$ under the velocity field in (4.4) with initial condition

$$\Gamma(0) = \{(x_1, x_2) : |x_1|^2 + 9|x_2|^2 = 1\}$$

by the direct method (i.e., mesh points move with velocity u) and the proposed method are presented in Figure 4.4. The proposed method significantly improves the mesh quality for this example again.

Example 4.4 (PDEs in a domain with moving boundary). In the last example, we demonstrate the effectiveness of the proposed method in combination of the arbitrary Lagrangian–Eulerian method for solving PDEs in a domain with a moving boundary, i.e., the parabolic equation

$$\partial_t \varphi - \Delta \varphi = f \tag{4.5}$$

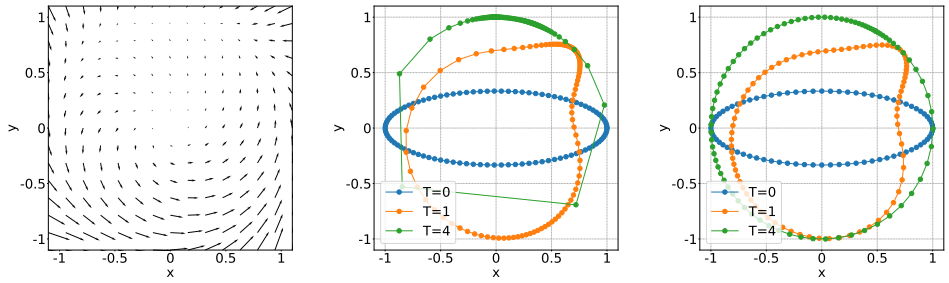

(a) The velocity field u (b) Evolution under velocity u (c) Evolution in our method

Fig. 4.4. *Evolution of a curve* $\Gamma(t)$ *under velocity field* u *(Example 4.3).*

in domain $\Omega(t)$ with its boundary $\Gamma(t) = \partial\Omega(t)$ evolving under the velocity field u in (4.4). By the arbitrary Lagrangian–Eulerian method, we solve the following reformulated equation:

$$\partial_t^\bullet \varphi - (w \cdot \nabla)\varphi + \Delta\varphi = f, \tag{4.6}$$

where w is the mesh velocity and $\partial_t^\bullet$ denotes the material derivative with respect to w. The mesh velocity in the bulk domain $\Omega(t)$ is obtained by a harmonic extension of the boundary velocity. Thus the direct method solves the bulk PDEs with boundary mesh points moving under velocity u, while the proposed method solves the bulk PDEs with boundary mesh points moving under a modified velocity with tangential motion determined by solving some boundary PDEs.

The influence of the proposed method on the mesh quality in the bulk domain can be clearly observed in Figure 4.5. Compared with solving PDEs in bulk domain, the computational cost of solving boundary PDEs is relatively small, as presented in Figure 4.6.

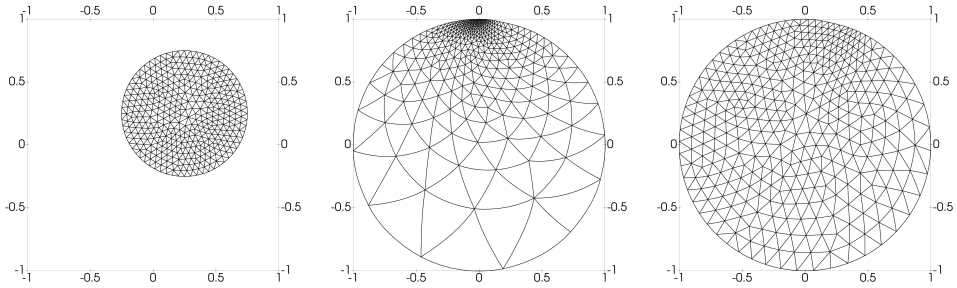

(a) The mesh at $t = 0$ (b) Mesh by the direct method (c) Mesh by proposed method

Fig. 4.5. *ALE moving mesh at* $t = 4$ *with finite elements of degree* $k = 3$.

The errors e_φ^E and e_φ^T of the numerical solutions up to time $T = 4$ given by the direct method and the proposed method, respectively, in approximating the exact solution $\varphi(x, t) = \log(2 + t) + \exp(x^2 + y^2)$ (with f and Dirichlet boundary condition determined by this exact solution), are presented in Figure 4.7. From Figures 4.6 and 4.7 we see that the proposed method is about 100 times more accurate than the direct

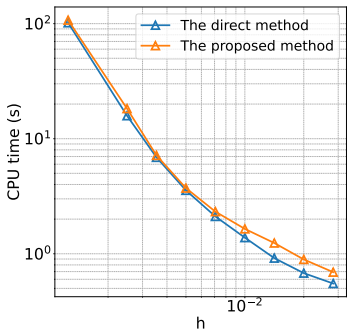

(a) CPU time per time step

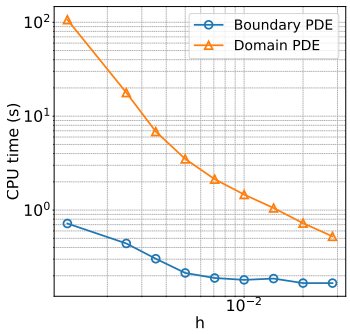

(b) Time for bulk and boundary PDEs

Fig. 4.6. *CPU time per time step for solving the bulk and boundary PDEs.*

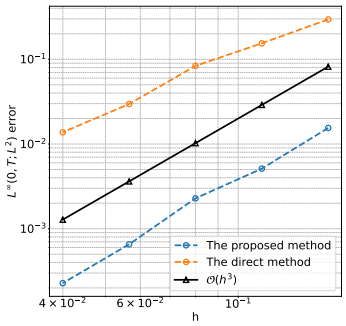

(a) Finite elements of degree $k = 2$

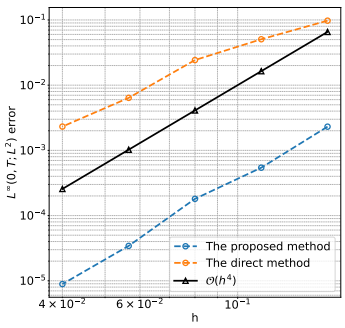

(b) Finite elements of degree $k = 3$

Fig. 4.7. $L^\infty(0,T;L^2)$ *errors of the numerical solutions to* (4.5).

method with roughly the same CPU time.

5. Conclusions. We have presented a novel evolving surface finite element method, by constructing an artificial tangential velocity based on novel equivalent formulation of the continuous problem, for computing the evolution of hypersurface under a smooth prescribed velocity field in $\mathbb{R}^d$, $d = 2, 3$. We have proved the stability and optimal-order convergence of the proposed method for finite elements of degree $k \geq 2$, and have illustrated the effectiveness of the constructed artificial tangential velocity in maintaining good mesh quality of the evolving surfaces through the numerical examples. Moreover, the application of the proposed method in solving PDEs in an evolving bulk domain has revealed the great benefit from the proposed method in decreasing the error of numerical solutions without essentially increasing the computational cost.

REFERENCES

[1] E. Bänsch, P. Morin, and R. Nochetto. A finite element method for surface diffusion: The parametric case. *J. Comput. Phys.*, 203(1):321–343, 2005.

[2] W. Bao, H. Garcke, R. Nürnberg, and Q. Zhao. Volume-preserving parametric finite element methods for axisymmetric geometric evolution equations. *J. Comput. Phys.*, 460:111180, 2022.

[3] J. W. Barrett, K. Deckelnick, and V. Styles. Numerical analysis for a system coupling curve evolution to reaction diffusion on the curve. *SIAM J. Numer. Anal.*, 55(2):1080–1100, 2017.
[4] J. W. Barrett, H. Garcke, and R. Nürnberg. A parametric finite element method for fourth order geometric evolution equations. *J. Comput. Phys.*, 222(1):441–467, 2007.
[5] J. W. Barrett, H. Garcke, and R. Nürnberg. On the parametric finite element approximation of evolving hypersurfaces in $\mathbb{R}^3$. *J. Comput. Phys.*, 227(9):4281–4307, 2008.
[6] J. W. Barrett, H. Garcke, and R. Nürnberg. Parametric approximation of Willmore flow and related geometric evolution equations. *SIAM J. Sci. Comput.*, 31(1):225–253, 2008.
[7] J. W. Barrett, H. Garcke, and R. Nürnberg. A variational formulation of anisotropic geometric evolution equations in higher dimensions. *Numer. Math.*, 109(1):1–44, 2008.
[8] J. W. Barrett, H. Garcke, and R. Nürnberg. Finite-element approximation of coupled surface and grain boundary motion with applications to thermal grooving and sintering. *European J. Appl. Math.*, 21:519–556, 2010.
[9] J. W. Barrett, H. Garcke, and R. Nürnberg. On stable parametric finite element methods for the Stefan problem and the Mullins-Sekerka problem with applications to dendritic growth. *J. Comput. Phys.*, 229:6270–6299, 2010.
[10] J. W. Barrett, H. Garcke, and R. Nürnberg. Numerical computations of faceted pattern formation in snow crystal growth. *Phys. Rev. E*, 86(1):011604, 2012.
[11] J. W. Barrett, H. Garcke, and R. Nürnberg. A stable parametric finite element discretization of two-phase Navier–Stokes flow. *J. Sci. Comput.*, 63(1):78-117, 2015.
[12] J. W. Barrett, H. Garcke, and R. Nürnberg. Parametric finite element approximations of curvature-driven interface evolutions. Handb. Numer. Anal., 21: 275-423, 2020.
[13] S. Bartels. A simple scheme for the approximation of the elastic flow of inextensible curves. *IMA J. Numer. Anal.*, 33(4):1115–1125, 2013.
[14] H. Benninghoff and H. Garcke. Segmentation of three-dimensional images with parametric active surfaces and topology changes. *J. Sci. Comput.*, 72(3):1333-1367, 2017.
[15] K. Deckelnick. Weak solutions of the curve shortening flow. *Calc. Var. Partial Differential Equations*, 5(6):489–510, 1997.
[16] K. Deckelnick, C. M. Elliott, and T. Ranner. Unfitted finite element methods using bulk meshes for surface partial differential equations. *SIAM J. Numer. Anal.*, 52(4):2137–2162, 2014.
[17] A. Demlow. Higher-order finite element methods and pointwise error estimates for elliptic problems on surfaces. *SIAM J. Numer. Anal.*, 47(2):805–827, 2009.
[18] G. Dziuk and C. Elliott. Finite elements on evolving surfaces. *IMA J. Numer. Anal.*, 27(2):262–292, 2007.
[19] G. Dziuk, D. Kröner, and T. Müller. Scalar conservation laws on moving hypersurfaces. *Interfaces Free Bound.*, 15(2):203–236, 2013.
[20] D. Edelmann. Finite element analysis for a diffusion equation on a harmonically evolving domain. *IMA J. Numer. Anal.*, 42(2):1866–1901, 2022.
[21] C. Elliott and H. Fritz. On approximations of the curve shortening flow and of the mean curvature flow based on the DeTurck trick. *IMA J. Numer. Anal.*, 37(2):543–603, 2017.
[22] C. M. Elliott and T. Ranner. Evolving surface finite element method for the Cahn-Hilliard equation. *Numer. Math.*, 129(3):483–534, 2015.
[23] C. M. Elliott and T. Ranner. A unified theory for continuous-in-time evolving finite element space approximations to partial differential equations in evolving domains. *IMA J. Numer. Anal.*, 41(3):1696–1845, 2021.
[24] C. M. Elliott and V. Styles. An ALE ESFEM for solving PDEs on evolving surfaces. *Milan J. Math.*, 80(2):469–501, 2012.
[25] C. M. Elliott and C. Venkataraman. Error analysis for an ALE evolving surface finite element method. *Numer. Methods Partial Differ. Equations*, 31(2):459–499, 2015.
[26] L. Formaggia and F. Nobile. A stability analysis for the Arbitrary Lagrangian Eulerian formulation with finite elements. *East-West J. Numer. Math.*, 7: 105-132, 1999.
[27] G. Fu. Arbitrary Lagrangian–Eulerian hybridizable discontinuous Galerkin methods for incompressible flow with moving boundaries and interfaces. *Comput. Methods Appl. Mech. Eng.*, 367:113158, 2020.
[28] D. Gilbarg and N. S. Trudinger. *Elliptic Partial Differential Equations of Second Order*. Classics in mathematics. Springer, second edition, 2001.
[29] W. Gong, B. Li, and Q. Rao. Convergent evolving finite element approximations of boundary evolution under shape gradient flow. *IMA J. Numer. Anal.*, 2023, accepted.
[30] J. Hu and B. Li. Evolving finite element methods with an artificial tangential velocity for mean curvature flow and Willmore flow. *Numer. Math.*, 152(1):127–181, 2022.
[31] G. Huisken. Flow by mean curvature of convex surfaces into spheres. *J. Differ. Geom.*, 20(1):237–266, 1984.
[32] S. Hysing, S. Turek, D. Kuzmin, N. Parolini, E. Burman, S. Ganesan, and L. Tobiska. Quanti-

tative benchmark computations of two-dimensional bubble dynamics. *Internat. J. Numer. Methods Fluids*, 60(11):1259–1288, 2009.

[33] T. Kemmochi, Y. Miyatake, and K. Sakakibara. Structure-preserving numerical methods for constrained gradient flows of planar closed curves with explicit tangential velocities, 2022, http://arxiv.org/abs/2208.00675.

[34] B. Kovács. High-order evolving surface finite element method for parabolic problems on evolving surfaces. *IMA J. Numer. Anal.*, 38(1):430–459, 2018.

[35] B. Kovács. Computing arbitrary Lagrangian Eulerian maps for evolving surfaces. *Numer. Methods Partial Differ. Equations*, 35(3):1093–1112, 2019.

[36] B. Kovács, B. Li, and C. Lubich. A convergent evolving finite element algorithm for mean curvature flow of closed surfaces. *Numer. Math.*, 143(4):797–853, 2019.

[37] B. Kovács, B. Li, and C. Lubich. A convergent evolving finite element algorithm for Willmore flow of closed surfaces. *Numer. Math.*, 149(3):595–643, 2021.

[38] B. Kovács, B. Li, C. Lubich and C. A. Power Guerra. Convergence of finite elements on an evolving surface driven by diffusion on the surface. *Numer. Math.*, 137(3): 643–689, 2017.

[39] B. Kovács and C. A. Power Guerra. Higher order time discretizations with ALE finite elements for parabolic problems on evolving surfaces. *IMA J. Numer. Anal.*, 38(1):460–494, 2018.

[40] R. Lan and P. Sun. A novel arbitrary Lagrangian-Eulerian finite element method for a parabolic/mixed parabolic moving interface problem. *J. Comput. Appl. Math.*, 383:113125, 2020.

[41] B. Li, Y. Xia, and Z. Yang. Optimal convergence of arbitrary Lagrangian-Eulerian iso-parametric finite element methods for parabolic equations in an evolving domain. *IMA J. Numer. Anal.*, 43:501–534, 2023.

[42] G. MacDonald, J.A. Mackenzie, M. Nolan, and R.H. Insall. A computational method for the coupled solution of reaction–diffusion equations on evolving domains and manifolds: Application to a model of cell migration and chemotaxis. *J. Comput. Phys.*, 309:207–226, 2016.

[43] G. MacDonald, C. Rowlatt, M. Nolan, and R. Insall. A conservative finite element ALE scheme for mass-conservative reaction-diffusion equations on evolving two-dimensional domains. *SIAM J. Sci. Comput.*, 43(1):B132–B166, 2021.

[44] A. Mierswa. Error estimates for a finite difference approximation of mean curvature flow for surfaces of torus type, PhD Thesis, Otto-von-Guericke-Universität, Magdeburg, 2020.

[45] M. A. Olshanskii and A. Reusken. A finite element method for surface PDEs: matrix properties. *Numer. Math.*, 114(3):491–520, 2010.

[46] T. Richter. *Fluid-Structure Interactions: Models, Analysis and Finite Elements*. Lecture Notes in Computational Science and Engineering. Springer International Publishing, 2017.

[47] T. Richter and T. Wick. Finite elements for fluid–structure interaction in ALE and fully Eulerian coordinates. *Comput. Methods Appl. Mech. Eng.*, 199(41):2633–2642, 2010.